

1 **Multi-functional foot use during running in the zebra-tailed** 2 **lizard (*Callisaurus draconoides*)**

3 Chen Li¹, S. Tonia Hsieh², and Daniel I. Goldman^{1*}

4 ¹*School of Physics, Georgia Institute of Technology, Atlanta, GA 30332, USA and*

5 ²*Department of Biology, Temple University, Philadelphia, PA 19122, USA*

6 *Author for correspondence (daniel.goldman@physics.gatech.edu)

7 **Summary**

8 **A diversity of animals that run on solid, level, flat, non-slip surfaces appear to bounce on**
9 **their legs; elastic elements in the limbs can store and return energy during each step. The**
10 **mechanics and energetics of running in natural terrain, particularly on surfaces that can**
11 **yield and flow under stress, is less understood. The zebra-tailed lizard (*Callisaurus***
12 ***draconoides*), a small desert generalist with a large, elongate, tendinous hind foot, runs**
13 **rapidly across a variety of natural substrates. We use high speed video to obtain detailed**
14 **three-dimensional running kinematics on solid and granular surfaces to reveal how leg, foot,**
15 **and substrate mechanics contribute to its high locomotor performance. Running at ~ 10**
16 **body length/s (~ 1 m/s), the center of mass oscillates like a spring-mass system on both**
17 **substrates, with only 15% reduction in stride length on the granular surface. On the solid**
18 **surface, a strut-spring model of the hind limb reveals that the hind foot saves about 40% of**
19 **the mechanical work needed per step, significant for the lizard's small size. On the granular**
20 **surface, a penetration force model and hypothesized subsurface foot rotation indicates that**
21 **the hind foot paddles through fluidized granular medium, and that the energy lost per step**
22 **during irreversible deformation of the substrate does not differ from the reduction in the**
23 **mechanical energy of the center of mass. The upper hind leg muscles must perform three**
24 **times as much mechanical work on the granular surface as on the solid surface to**
25 **compensate for the greater energy lost within the foot and to the substrate.**

26 Key words: terrestrial locomotion, mechanics, energetics, kinematics, spring-mass system, elastic
27 energy savings, dissipation, granular media

28 Running title: Substrate effects on foot use in lizards

30

Introduction

31 Rapid locomotion like running and hopping can be modeled as a spring-mass system bouncing in
32 the sagittal plane (i.e., the Spring-Loaded Inverted Pendulum model, SLIP) (Blickhan, 1989).
33 This has been demonstrated in a variety of animals (Blickhan and Full, 1993; Holmes et al., 2006)
34 in the laboratory on rigid, level, flat, non-slip surfaces (hereafter referred to as “solid surfaces”)
35 such as running tracks and treadmills (Dickinson et al., 2000). In the SLIP model, the animal
36 body (represented by the center of mass, CoM) bounces on a single leg (represented by a spring)
37 like a pogo stick, and exerts point contact on the solid ground. The leg spring compresses during
38 the first half of stance, and then recoils during the second half of stance. Through this process, the
39 mechanical (i.e., kinetic plus gravitational potential) energy of the CoM is exchanged with elastic
40 energy stored in the compressed leg spring, reducing energy use during each step. For animals
41 like insects (e.g., Schmitt et al., 2002) and reptiles (e.g., Chen et al., 2006) that run with a
42 sprawled limb posture, the CoM also oscillates substantially in the horizontal plane in a similar
43 fashion, which can also be modeled as a spring-mass system bouncing in the horizontal plane (i.e.,
44 the Lateral Leg Spring model, LLS) (Schmitt et al., 2002). Both the SLIP and the LLS models
45 predict that the mechanical energy of the CoM is lowest at mid-stance and highest during aerial
46 phase.

47 In these models, the spring-mass system and the interaction with the solid ground are perfectly
48 elastic and do not dissipate energy; thus no net work is performed. However, as animals move
49 across natural surfaces, energy is dissipated both within their body and limbs (Fung, 1993) and to
50 the environment (Dickinson et al., 2000). Therefore, mechanisms to reduce energy loss during
51 locomotion can be important. The limbs of many organisms possess elastic elements such as
52 tendons and ligaments that can function as springs to store and return energy during rapid
53 locomotion like running and hopping to decrease energetic cost (Alexander, 2003). Most notable
54 for this function are the ankle extensor tendons in the lower hind leg and the digital flexor
55 tendons and ligaments in the lower fore leg (Alexander, 2003). Furthermore, different limb-
56 ground interaction strategies may be utilized depending on the dissipative properties of the
57 substrate.

58 Laboratory experiments have begun to reveal mechanisms of organisms running on non-solid
59 substrates, such as elastic (Ferris et al., 1998; Spence et al., 2010), damped (Moritz and Farley,
60 2003), inclined (Roberts et al., 1997), or uneven (Daley and Biewener, 2006; Sponberg and Full,
61 2008) surfaces; surfaces with few footholds (Spagna et al., 2007); and the surface of water
62 (Glasheen and McMahon 1996a; Hsieh, 2003). While spring-mass-like CoM motion was

63 observed only in some of these studies (Ferris et al., 1998; Moritz and Farley, 2003; Spence et al.,
64 2010), a common finding is that on non-solid surfaces limbs do not necessarily behave like
65 springs to save energy. In addition, these studies suggest that both the active control of body and
66 limb movement through the nervous system, and the passive mechanical responses of
67 viscoelastic limbs and feet with the environment, play important roles in the control of rapid
68 terrestrial locomotion (for reviews, see Full and Koditschek, 1999; Dickinson et al., 2000).

69 Many substrates found in nature, such as sand, gravel, rubble, dirt, soil, mud, and debris, can
70 yield and flow under stress during locomotion and experience solid-fluid transitions, through
71 which energy may be dissipated via plastic deformation. Understanding locomotion on these
72 substrates is challenging in part because, unlike for flying and swimming where the fluid flows
73 and forces can in principle be determined by solving the Navier-Stokes equations in the presence
74 of moving boundary conditions (Vogel, 1996), no comprehensive force models yet exist for
75 terrestrial substrates that yield and flow (hereafter referred to as “flowing substrates”).

76 Granular materials (Nedderman, 1992) like desert sand which are composed of similarly sized
77 particles provide a good model substrate for studying locomotion on flowing substrates.
78 Compared to other flowing substrates, granular materials are relatively simple and the intrusion
79 forces within them can be modeled empirically (Hill et al., 2005). Their mechanical properties
80 can also be precisely and repeatedly controlled using a fluidized bed (Li et al., 2009). In addition,
81 locomotion on granular surfaces is directly relevant for many desert-dwelling reptiles and
82 arthropods such as lizards, snakes, and insects (Mosauer, 1932; Crawford, 1981). Recent
83 advances in the understanding of force and flow laws in granular materials subject to localized
84 intrusion (Hill et al., 2005; Katsuragi and Durian, 2007; Gravish et al., 2010; Ding et al., 2011a)
85 begin to provide insight into the mechanics of locomotion on (and within) granular substrates (Li
86 et al., 2009; Maladen et al., 2009; Mazouchova et al., 2010; Li et al., 2010b; Maladen et al., 2011;
87 Ding et al., 2011b; Li et al., in press).

88 The zebra-tailed lizard (*Callisaurus draconoides*, SVL ~ 10 cm, mass ~ 10 g, Fig. 1A) is an
89 excellent model organism for studying running on natural surfaces, because of its high locomotor
90 performance over diverse terrain. As a desert generalist, this lizard lives in a range of desert
91 habitats including flat land, washes, and sand dunes (Vitt and Ohmart, 1977; Korff and McHenry,
92 2011), and encounters a large variety of substrates ranging from rocks, gravel, closely-packed
93 coarse sand, and loosely-packed fine sand (Karasov and Anderson, 1998; Korff and McHenry,
94 2011). The zebra-tailed lizard is the fastest-running species among desert lizards of similar size

95 (Irschick and Jayne, 1999a), and has been observed to run at up to 4 m/s (50 bl/s) both on solid
96 (e.g., treadmill) (Irschick and Jayne, 1999a) and on granular (e.g., sand dunes) (Irschick and
97 Jayne, 1999b) surfaces. Its maximal acceleration and running speed also did not differ
98 significantly when substrate changes from coarse wash sand to fine dune sand, whose yield
99 strengths differ by a factor of three (Korff and McHenry, 2011).

100 Of particular interest is whether and how the zebra-tailed lizard's large, elongate hind foot
101 contributes to its high locomotor capacity. In addition to a slim body, a long tapering tail, and
102 slender legs (Fig. 1A), the zebra-tailed lizard has an extremely large, elongate hind foot, the
103 largest (40% SVL) among lizards of similar size (Irschick and Jayne, 1999a). Its hind foot is
104 substantially larger than the fore foot (area = 1 cm² vs. = 0.3 cm²) and likely plays a dominant role
105 for locomotion (Mosauer, 1932). Recent studies in insects, spiders, and geckos (Jindrich and Full,
106 1999; Antumn et al., 2000; Dudek and Full, 2006; Spagna et al., 2007) suggested that animals can
107 rely on appropriate morphology and material properties of their bodies and limbs to accommodate
108 variable, uncertain conditions during locomotion. Despite suggestions that the large foot area
109 (Mosauer, 1932) and increased stride length via elongate toes may confer locomotor advantages
110 (Irschick and Jayne, 1999a), the mechanisms of how the hind foot contributes to the zebra-tailed
111 lizard's high running capacity remain unknown.

112 In this paper, we study the mechanics and mechanical energetics of the zebra-tailed lizard running
113 on two well-defined model surfaces, a solid surface and a granular surface. These two surfaces lie
114 on opposite ends of the spectrum of substrates that the zebra-tailed lizard encounters in its natural
115 environment, and present distinct conditions for locomotion. We investigate whether the lizard's
116 center of mass bounces like a spring-mass system during running on both solid and granular
117 surfaces. We combine measurements of three-dimensional kinematics of the lizard's body, hind
118 limb, and hind foot, dissection and resilience measurements of the hind limb, and modeling of
119 foot-ground interactions on both substrates, and demonstrate that the lizard's large, elongate hind
120 foot serves different functions during running on solid and granular surfaces. We find that on the
121 solid surface, the hind foot functions as an energy-saving spring; on the granular surface, it
122 functions as a dissipative, force-generating paddle to generate sufficient lift during each step. The
123 larger energy dissipation to the substrate and within the foot during running on the granular
124 surface must be compensated for by greater mechanical work done by the upper hind leg muscles.

125

126

Materials and methods

127

Animals

128 Seven adult zebra-tailed lizards (*Callisaurus draconoides*) were collected from the Mojave Desert,
129 AZ, USA in 08/2007 (Permit SP591773) for three-dimensional kinematics experiments. Table 1
130 shows the morphological measurements for these seven animals. Eleven additional adult animals
131 were collected from the Mojave Desert, CA, USA in 09/2009 (Permit SC 10901) for hind limb
132 resilience measurements. Two preserved specimens were used for dissection. The animals were
133 housed in the Physiological Research Laboratory animal facility of The Georgia Institute of
134 Technology. Each animal was housed individually in an aquarium filled with sand, and fed
135 crickets and mealworms dusted with vitamin and calcium supplement two to three times a week.
136 The ambient temperature was maintained at 28°C during the day and 24°C during the night. Full-
137 spectrum fluorescent bulbs high in UVB were set to a 12 hour/12 hour light/dark schedule.
138 Ceramic heating elements were provided 24 hours a day to allow the animals to thermo-regulate
139 at preferred body temperature. All experimental procedures were conducted in accordance with
140 The Georgia Institute of Technology IACUC protocols.

141

Surface treatments

142 A wood board ($120 \times 23 \times 1 \text{ cm}^3$) bonded with sandpaper (grit size $\sim 0.1 \text{ mm}$) for enhanced
143 traction was used as the solid surface. Glass particles (diameter = $0.27 \pm 0.04 \text{ mm}$ mean ± 1
144 standard deviation, density = $2.5 \times 10^3 \text{ kg/m}^3$, Jaygo Incorporated, Union, NJ, USA) were used as
145 the granular substrate, which are approximately spherical and of similar size to typical desert sand
146 (Dickinson and Ward, 1994). Before each trial, a custom-made fluidized bed trackway (200 cm
147 long, 50 cm wide) prepared the granular substrate (12 cm deep) into a loosely packed state
148 (volume fraction = 0.58) for repeatable yield strength (for experimental details of the fluidized
149 bed trackway, see Li et al., 2009).

150

Three-dimensional kinematics

151 We used high speed video to obtain three-dimensional kinematics as the lizard ran across the
152 prepared surfaces (Fig. 1B). Before each session, high-contrast markers (Wite-Out, Garden Grove,
153 CA, USA) were painted on each animal for digitizing at nine joints along the midline of the trunk
154 and the right hind limb (Fig. 1A,B): neck (N), center of mass (CoM), pelvis (P), hip (H), knee (K),
155 ankle (A); and the metatarsal-phalangeal joint (MP), distal end of the proximal phalanx (PP), and
156 digit tip (T) of the fourth toe. The approximate longitudinal location of the CoM in resting
157 position was determined by tying a thread around the body of an anesthetized lizard and

158 repositioning the thread until the body balanced horizontally. Before each trial, the surface was
159 prepared (for the granular surface treatment only), and calibration images were taken of a custom-
160 made 39-point calibration object (composed of LEGO, Billund, Denmark). The animal was then
161 induced to run across the field of view by a slight tap or pinch on the tail. Two synchronized AOS
162 high speed cameras (AOS Technologies, Baden Daettwil, Switzerland) captured simultaneous
163 dorsal and lateral views at 500 frame/s (shutter time = 300 μ s). The ambient temperature was
164 maintained at 35°C during the test. Animals were allowed to rest at least five minutes between
165 trials and at least two days between sessions.

166 We digitized the calibration images and high speed videos, and used direct linear transformation
167 (DLT) to reconstruct three-dimensional kinematics from the two-dimensional kinematics from
168 both dorsal and lateral views. Digitization and DLT calculations were performed using custom
169 software (DLTcal5 and DLTdv5, Hedrick, 2008). Axes were set such that +x pointed in the
170 direction of forward motion, +z pointed vertically upward, and +y pointed to the left of the animal.
171 Footfall patterns of touchdown and takeoff were determined from the videos. On the granular
172 surface, because the hind foot often remained obscured by splashed grains during foot extraction,
173 we defined foot takeoff as when the knee began to flex following extension during limb
174 protraction (which is when foot takeoff occurs on the solid surface). To reduce noise and enable
175 direct comparisons among different running trials, position data were filtered with a Butterworth
176 low-pass filter with a cutoff frequency of 75 Hz, and interpolated to 0–100% of one full stride
177 period (T) between two successive touchdowns of the right hind limb. All data analysis was
178 completed with MATLAB (MathWorks, Natick, MA, USA) unless otherwise specified.

179 *Statistics*

180 We accepted trials that met the following criteria: the animal ran continuously through the field of
181 view, the run was straight without contacting sidewalls of the trackway, there was a full stride
182 (between two consecutive touchdowns of the right hind limb) in the range of view, all the nine
183 markers were visible throughout the full stride, and the forward speed changed less than 20%
184 after the full stride. With these criteria, out of a total of 125 trials from 7 individuals on both solid
185 (61 trials from 7 individuals) and granular (64 trials from 7 individuals) surfaces collected over a
186 period of over three months, we ultimately accepted 51 runs from 7 individuals on solid (23 runs
187 from 7 individuals) and granular (28 runs from 7 individuals) surfaces. Because the data set had
188 an unequal number of runs per individuals, and because we were measuring freely-running
189 animals and did not control for speed, to maintain statistical power, all statistical tests were

190 performed on a subset of these data using one representative run per individual on both solid ($N =$
191 7) and granular ($N = 7$) surfaces. The representative run for each individual was selected based on
192 having the most consistent running speed for at least one full stride and was also closest to the
193 mean running speed of all 51 trials. Data are reported as mean \pm 1 standard deviation (s.d.) from
194 the 7 representative runs on each substrate unless otherwise specified.

195 To determine the effect of substrate, all kinematic variables were corrected for size-related
196 differences by regressing the variables against SVL and taking the residuals for those that
197 regressed significantly with SVL ($P < 0.05$). We then ran an ANCOVA with substrate and speed
198 as covariates to test for substrate effects, independent of running speeds. All statistical tests were
199 performed using JMP (SAS, Cary, NC, USA).

200 For the energetics data, we used dimensionless quantities by normalizing energies of each run to
201 the CoM mechanical energy at touchdown of that run, thus eliminating the effect of mass and
202 running speed on energies. An ANOVA was used to test the differences between the reduction in
203 CoM mechanical energy, elastic energies, and energy loss. A Tukey's HSD was used for post-hoc
204 tests where needed.

205 *Dissection and model of hind limb*

206 To gain insight into the role of anatomical components of the hind limb on mechanics during
207 locomotion, we dissected the hind limb of two preserved specimens. We quantified anatomical
208 dimensions by measuring the radii of the knee (K), ankle (A), the metatarsal-phalangeal joint
209 (MP), the distal end of the proximal phalanx (PP), and the digit tip (T) of the fourth toe. We also
210 observed the muscle and tendon arrangements within the lower leg and the foot. Based on these
211 anatomical features, we developed a model of the hind limb which incorporated the structure,
212 properties, and function of its main elements.

213 *Resilience measurements of hind limb*

214 To characterize the resilience of the hind limb for estimation of energy return, a modification of
215 the work loop technique was used (Fig. 2A), in which the limb was kept intact and forces were
216 applied to the whole limb instead of a single muscle (Dudek and Full, 2006). The animal was
217 anesthetized using 2% isoflurane air solution during the test. The hind foot was maintained within
218 the vertical plane, pushed down onto and then extracted from a custom force platform suited for
219 small animals ($10.2 \times 7.6 \text{ cm}^2$, range = 2.5 N, resolution = 0.005 N) bonded with sandpaper (grit
220 size $\sim 0.1 \text{ mm}$). Ground reaction force F was measured at 10 kHz sampling rate using a custom

221 LabVIEW program (National Instruments, Austin, TX, USA). A Phantom high speed camera
222 (Vision Research, Wayne, NJ, USA) simultaneously recorded deformation of the foot from the
223 side view at 250 frame/s (shutter time = 500 μ s). High-contrast markers (Wite-Out, Garden Grove,
224 CA, USA) were painted on the joints of the hind foot (A, MP, PP, T, and a point on the tibia
225 above the ankle). The ambient temperature was maintained at 35°C during the test.

226 Videos of foot deformation were digitized to obtain the angular displacement of the foot $\Delta\theta =$
227 $\theta_0 - \theta_t$, i.e., the change in the angle formed by the tibia and the foot (from the ankle to the digit tip
228 of the fourth toe) (Fig. 2A). Angular displacement $\Delta\theta$ was synchronized with the measured torque
229 τ about the ankle (calculated from the measured ground reaction force) to obtain a passive work
230 loop. The damping ratio of the hind limb, i.e., the percentage of energy lost within the hind limb
231 after loading and unloading, was calculated as the fraction of area within a work loop relative to
232 the area under the higher loading curve (Fung, 1993). Hind limb resilience, i.e., the percentage of
233 energy returned by the foot after loading and unloading, was one minus the damping ratio (Ker et
234 al., 1987; Dudek and Full, 2006). An ANOVA was used to test the effect of maximal torque,
235 maximal angular displacement, loading rate, and individual animal on hind limb resilience.

236 *Granular penetration force measurements*

237 While comprehensive force models are still lacking to calculate ground reaction forces during
238 locomotion granular media, a low speed penetration force model was previously used to explain
239 the locomotor performance of a legged robot on granular media (Li et al., 2009). Similarly, to
240 estimate the vertical ground reaction force on the lizard foot during running on the granular
241 surface, we measured the vertical force on a plate slowly penetrating vertically into the granular
242 substrate (Fig. 2B). Before each trial, a fluidized bed (area = 24 \times 22 cm²) prepared the granular
243 substrate (depth = 12 cm) into a loosely packed state (volume fraction = 0.58) (for details, see
244 Maladen et al., 2009). A robotic arm (CRS robotics, Burlington, OT, Canada) pushed a
245 horizontally-oriented plate vertically downward at 0.01 m/s into the granular substrate to a depth
246 of 7.6 cm, and then extracted the plate vertically at 0.01 m/s. The force on the plate was measured
247 by a force transducer (ATI Industrial Automation, Apex, NC, USA) mounted between the robotic
248 arm and the plate at 100 Hz sampling rate using a custom LabVIEW program (National
249 Instruments, Austin, TX, USA). The depth of the plate was measured by tracking the position of
250 an LED light marker mounted on the robotic arm in side view videos taken by a Pike high speed
251 camera (Edmund Optics, Barrington, NJ, USA). Two thin aluminum plates of different area were

252 used ($A_1 = 7.6 \times 2.5 \text{ cm}^2$ and $A_2 = 3.8 \times 2.5 \text{ cm}^2$; thickness = 0.6 cm). Three trials were performed
253 for each plate.

254

255

Results

256

Performance and gait

257 On both solid and granular surfaces, the zebra-tailed lizard ran with a diagonal gait, a sprawled
258 limb posture, and lateral trunk bending (see Fig. 3 and Movies 1, 2 in supplementary material for
259 representative runs on both substrates). Figure 4 shows average forward speed $\bar{v}_{x,\text{CoM}}$, stride
260 frequency f , and duty factor D of the entire data set (all symbols; 23 runs on the solid surface and
261 28 runs on the granular surface) and of the representative runs (filled symbols; $N = 7$ on the solid
262 surface and $N = 7$ on the granular surface). Table 2 lists mean values and statistical results for all
263 the gait and kinematic variables from the representative runs for both solid ($N = 7$) and granular
264 ($N = 7$) surfaces. On both surfaces, $\bar{v}_{x,\text{CoM}}$ increased with f (Fig. 4A, $P < 0.05$, ANCOVA), and D
265 decreased with $\bar{v}_{x,\text{CoM}}$ (Fig. 4B, $P < 0.05$, ANCOVA). $D \approx 0.45$ on both surfaces resulting in an
266 aerial phase of approximately 5% stride period T between alternating stances (Fig. 5A). Neither
267 $\bar{v}_{x,\text{CoM}}$ ($P > 0.05$, ANOVA) nor D ($P > 0.05$, ANCOVA) significantly differ between surfaces.
268 Average stride length $\lambda = \bar{v}_{x,\text{CoM}}/f$ was 15% shorter on the granular surface ($P < 0.05$, ANCOVA).

269

Center of mass kinematics

270 The lizard displayed qualitatively similar center of mass oscillations during running on both
271 surfaces. The CoM forward speed $v_{x,\text{CoM}}$ (Fig. 5B) and vertical position z_{CoM} (Fig. 5C) oscillated at
272 $2f$, dropping during the first half and rising during the second half of a stance, i.e., reaching
273 minimum at mid-stance and maximum during the aerial phase. The CoM also oscillated medio-
274 laterally at f (Fig. 5D). Throughout the entire stride, z_{CoM} was significantly higher on the solid
275 surface ($P < 0.05$, ANCOVA). The CoM vertical oscillations Δz_{CoM} and lateral oscillations Δy_{CoM}
276 did not differ between substrates ($P > 0.05$, ANCOVA).

277

Hind foot, hind leg, and trunk kinematics

278 The lizard displayed distinctly different hind foot, hind leg, and trunk kinematics during running
279 on solid and granular surfaces (Figs. 3, 6). On the solid surface, the lizard used a digitigrade foot
280 posture (Fig. 3A–E, solid line/curve). During the entire stride, the hind foot engaged the solid

281 surface only with the digit tips. At touchdown, the toes were straight and pointed slightly
282 downward. The touchdown foot angle (measured along the fourth toe) was $\theta_{\text{touchdown}} = 12 \pm 4^\circ$
283 relative to the surface (Fig. 3A,E; Fig. 6A, red). During stance, the long toes pivoted over the
284 stationary digit tips (Fig. 3A–C, vertical dotted line shows zero displacement) and hyperextended
285 into a c-shape (Fig. 3B, solid curve). The foot straightened again at takeoff, pointing downward
286 and slightly backward (Fig. 3C, solid line), and then flexed during swing (Fig. 3D, solid curve).

287 On the granular surface, the lizard used a plantigrade foot posture (Fig. 3F,J, solid line). At
288 touchdown, the hind foot was nearly parallel with the surface, with the toes spread out and held
289 straight. In the vertical direction, the foot impacted the granular surface at speeds of up to 1 m/s.
290 The ankle joint slowed down to ~ 0.1 m/s within a few milliseconds following impact (a few
291 percent of stride period T) while the the foot started penetrating the surface. The touchdown foot
292 angle was $\theta_{\text{touchdown}} = 4 \pm 3^\circ$ relative to the surface (Fig. 3J; Fig. 6A, blue), significantly smaller
293 than that on the solid surface ($P < 0.05$, ANCOVA). During stance, the entire foot moved
294 subsurface and was obscured (Fig. 3G). The ankle joint remained visible right above the surface
295 and moved forward by about a foot length (Fig. 3F–H, vertical dotted line shows ankle
296 displacement). The foot was extracted from the substrate at takeoff, pointing downward and
297 slightly backward, and then flexed during swing (Fig. 3I, solid curve).

298 As a result of foot penetration on the granular surface, both the knee height z_{knee} (Fig. 6B) and
299 pelvis height z_{pelvis} (Fig. 6C) were lower on the granular surface ($P < 0.05$, ANCOVA). In addition,
300 on the granular surface, the knee moved downward by a larger vertical displacement Δz_{knee} during
301 the first half of stance ($P < 0.05$, ANCOVA; Fig. 6B), while the knee joint extended by a larger
302 angle $\Delta\theta_{\text{knee}}$ during the second half of stance ($P < 0.05$, ANCOVA; Fig. 6D). Throughout the
303 entire stride, the trunk was nearly horizontal on the solid surface (Fig. 3A–D, dashed line), but
304 pitched head-up on the granular surface (Fig. 3F–I, dashed line; Fig. 6E). On both surfaces, the
305 hind legs were sprawled at an angle of $\theta_{\text{sprawl}} \approx 40^\circ$ during stance (Fig. 3; θ_{sprawl} is defined as the
306 angle between the horizontal plane and the leg orientation in the posterior view). In most runs, the
307 tail was farther from the solid surface and closer to the granular surface (Fig. 3).

308 *Hind limb anatomy*

309 From morphological measurements (Table 1), the hind foot of the zebra-tailed lizard comprised
310 42% of the hind limb length, and the longest fourth toe alone accounted for 63% of the hind foot
311 length. These ratios are in similar range to previous observations (Irschick and Jayne, 1999a). The

312 slender foot had a cross-sectional radius of $r = 0.50\text{--}1.25$ mm tapering distally, with reducing
313 joint radii: $r_K = r_A = 1.25$ mm, $r_{MP} = 0.75$ mm, $r_{PP} = r_T = 0.50$ mm.

314 Unlike many cursorial mammals whose ankle extensor muscles of the lower hind leg have long
315 tendons (Alexander, 2003), ankle extensor tendons are nearly non-existent in the zebra-tailed
316 lizard (Fig. 7A). Instead, layers of elongate tendons were found in both the dorsal and ventral
317 surfaces of the foot. Our anatomical description is focused on the ventral muscle and tendon
318 anatomy in the hind limb and terms given to muscles and tendons follow (Russell, 1993). A large,
319 tendinous sheath, the superficial femoral aponeurosis, originates from the femoro-tibial
320 gastrocnemius, stretches across the ventral surface of the foot, and inserts on the metatarsal-
321 phalangeal joints for digits III and IV. The superficial portion of the femoro-tibial gastrocnemius
322 muscle body extends to the base of the ankle, thereby rendering the human equivalent of the
323 ankle extensor tendons (i.e., the “Achilles” tendon) absent. Deep to the superficial femoral
324 aponeurosis lie the flexor digitorum brevis muscles (not shown) which control the flexion of each
325 of the digits. Tendons from the flexor digitorum longus muscle located on the lower hind leg run
326 deep to the flexor digitorum brevis muscle bodies, and extend to the tips of the digits. No
327 additional tendons are visible deep to the flexor digitorum longus tendons.

328 *Hind limb model*

329 Based on the observed muscle and tendon anatomy, we propose a two-dimensional strut-spring
330 model of the hind limb (Fig. 7B), which assumes isometric contraction for the lower leg muscles
331 and incorporates the spring nature of the foot tendons. This model is inspired from previous
332 observations in large running and hopping animals of the strut-like function of ankle extensor
333 muscles (Biewener, 1998a; Roberts et al., 1997) and spring-like function of ankle extensor
334 tendons (for a review, see Alexander, 2003). Rigid segments (Fig. 7B, dashed lines), which are
335 free to rotate about joints within a plane, represent the skeleton. The ankle extensor muscles in the
336 lower leg, which originate on the femur and run along the ventral side of the tibia, are modeled as
337 a rigid strut (muscle strut, Fig. 7B, blue line) that contracts isometrically during stance in running.
338 A linear spring (tendon spring, Fig. 7B, red line), which originates from the distal end of the
339 muscle strut and extends to the digit tip, models the elastic foot tendons. The muscle strut and
340 tendon spring are ventrally offset from the midline of the skeleton at each joint by respective joint
341 radii.

342 *Hind limb resilience*

343 Representative passive work loops (Fig. 8A–C) showed that torque τ was higher when the foot
344 was pushed down on the solid surface than when it was extracted, similar to previous
345 observations in humans (Ker et al., 1987) and cockroaches (Dudek and Full, 2006). Maximal
346 torque was positively correlated with maximal angular displacement ($F_{1,62} = 64.3188$, $P < 0.001$,
347 ANOVA). The kinks observed in the middle of the loading curve were due to the fifth toe
348 contacting the surface. Average hind limb resilience calculated from the work loops was $R = 0.44$
349 ± 0.12 (Fig. 8D–F, 3 individuals, 64 trials). R did not differ between individuals ($F_{2,61} = 2.1025$, P
350 $= 0.1309$, ANOVA), and did not depend on maximal torque ($F_{1,62} = 0.5208$, $P = 0.4732$, ANOVA;
351 Fig. 8D), maximal angular displacement ($F_{1,62} = 0.0164$, $P = 0.8987$, ANOVA; Fig. 8E), or
352 average loading rate ($F_{1,62} = 1.1228$, $P = 0.2934$, ANOVA; Fig. 8F).

353 *Hind foot curvature, tendon deformation, and tendon stiffness*

354 The observed three-dimensional positions of the hind limb fit well to the two-dimensional hind
355 limb model (Fig. 9A–D), and enabled calculation of the curvature, tendon deformation, and
356 tendon stiffness of the hind foot (see Appendix). Calculated hind foot curvature κ (Fig. 9E, solid
357 curve) showed that the hind foot hyperextended during stance (positive κ) and flexed during
358 swing (negative κ). The foot was straight at touchdown and shortly after takeoff ($\kappa = 0$).
359 Calculated tendon spring deformation Δl (Fig. 9E, dashed curve) showed that the tendon spring
360 stretched during the first half and recoiled during the second half of stance. The estimated tendon
361 spring stiffness was $k = 4.4 \times 10^3$ N/m (see Appendix).

362 *Mechanical energetics on solid surface*

363 Using the observed CoM and hind limb kinematics, calculated tendon spring stiffness and
364 deformation, and measured hind limb resilience, we examined the mechanical energetics of the
365 lizard running on the solid surface (Table 3, Fig. 9F). From the observed CoM kinematics, in the
366 first half of stance, the mechanical energy of the CoM (kinetic energy plus gravitational potential
367 energy) decreased significantly from $E_{\text{touchdown}} = 1.00 \pm 0.00$ at touchdown to $E_{\text{mid-stance}} = 0.81 \pm$
368 0.08 at mid-stance ($F_{2,18} = 12.2345$, $P = 0.0004$, ANOVA, Tukey HSD). In the second half of
369 stance, the mechanical energy of the CoM recovered to $E_{\text{aerial}} = 0.95 \pm 0.10$ at mid aerial phase,
370 not significantly different from $E_{\text{touchdown}}$ (Tukey HSD). The reduction in CoM mechanical energy
371 in the first half of stance $\Delta E_{\text{mech}} = 0.19 \pm 0.08$ is the mechanical work needed per step on the solid
372 surface. Note that the energies of each run were normalized to $E_{\text{touchdown}}$ of that run.

373 At mid-stance, the elastic energy stored in the tendon spring was $E_{\text{storage}} = 0.18 \pm 0.13$ (calculated
374 from $1/2 k\Delta l_{\text{max}}^2$, see Appendix), not significantly different from ΔE_{mech} ($F_{1,12} = 0.0475$, $P =$
375 0.8312 , ANOVA). Because hind limb resilience $R = 0.44 \pm 0.12$, the elastic recoil of the foot
376 tendons returned an energy of $E_{\text{return}} = RE_{\text{storage}} = 0.08 \pm 0.06$, or $41 \pm 33\%$ of the mechanical work
377 needed per step (ΔE_{mech}) on the solid surface. We verified that foot flexion during swing induced
378 little energy storage ($< 0.1 E_{\text{storage}}$) because the hind foot was less stiff during flexion (0.7×10^3
379 N/m) than during hyperextension (4.4×10^3 N/m).

380 *Granular penetration force model*

381 Although little is known about the kinematics and mechanics of the complex limb intrusions
382 during legged locomotion on granular surfaces, we took inspiration from previous observations
383 that horizontal drag (Maladen et al., 2009) and vertical impact (Katsuragi and Durian, 2007)
384 forces in glass particles were insensitive to speed when intrusion speed was below approximately
385 0.5 m/s. Because the kinematics observed on the granular surface suggest that the vertical speeds
386 of most of the foot relative to the ground were below 0.5 m/s during most of the stance phase (see
387 Appendix), we assumed that the ground reaction forces on the lizard's feet were also insensitive
388 to speed. This allowed us to use the vertical penetration force measured at 0.01 m/s to model and
389 estimate the vertical ground reaction forces on the lizard foot.

390 From the force data on both plates (Fig. 10), vertical ground reaction force F_z was proportional to
391 both penetration depth $|z|$ and projected area A of the plate (area projected into the horizontal
392 plane). F_z was pointing upward during foot penetration, and pointing downward during foot
393 extraction and dropped by an order of magnitude. These measurements were in accord with
394 previous observations of forces on a sphere penetrating into granular media (Hill et al., 2005).
395 Furthermore, we estimated from free falling of particles under gravity that it would take longer
396 than the stance duration (45 ms) for the grains surrounding a penetrating foot to refill a hole
397 created by the foot of maximal depth ($|z|_{\text{max}} = 1.0$ cm, see Appendix). Thus we assumed that the
398 vertical ground reaction forces were negligible during foot extraction.

399 Therefore, we approximate the vertical penetration force as:

$$400 \quad F_z = \begin{cases} \alpha |z| A, & \text{for increasing } |z|, \\ 0, & \text{for decreasing } |z|, \end{cases} \quad (1)$$

401 where α is the vertical stress per unit depth, which is determined by the properties of the granular
402 material and increases with compaction (Li et al., 2009). Fitting $F_z = \alpha |z| A$ to the force data

403 during penetration over regions where the plate was fully submerged and far from boundary (Fig.
404 10, dashed lines), we obtained $\alpha = 3.5 \times 10^5 \text{ N/m}^3$ for loosely packed $0.27 \pm 0.04 \text{ mm}$ diameter
405 glass particles.

406 *Vertical ground reaction force on granular surface*

407 During a stance on the granular surface, the CoM vertical speed $v_{z,\text{CoM}}$ (calculated from z_{CoM}) was
408 approximately sinusoidal (Fig. 11A, dashed curve). This implies that the F_z on a lizard foot must
409 be approximately sinusoidal. In addition, the foot was nearly horizontal at touchdown, but pointed
410 downward and slightly backward during takeoff. In consideration of the functional form of the
411 penetration force (Eqn. 1), we hypothesized that during stance the foot rotated subsurface by $\pi/2$
412 in the sagittal plane (Fig. 11C), increasing foot depth $|z|$ but decreasing projected foot area A , thus
413 resulting in a sinusoidal F_z which reaches a maximum at mid-stance before the foot reaches
414 largest depth (see Appendix). A sinusoidal F_z is also possible for a fixed projected foot area if the
415 foot maintains contact on solidified grains. However, this is unlikely considering that during
416 stance the ankle moved forward at the surface level by a foot length.

417 Assuming that during stance the hind foot rotated by $\pi/2$ in the sagittal plane at a constant angular
418 velocity, the vertical ground reaction force that each foot generated was $F_z = 5\pi mg/9 \sin 10\pi t/9T$
419 (see Appendix). The net vertical acceleration due to this F_z and the animal weight mg was $a_z =$
420 $F_z/m - g$ (Fig. 11B; solid and dashed curves are a_z from both hind feet, shifted from each other by
421 $T/2$). The CoM vertical speed $v_{z,\text{CoM}}$ predicted from the total a_z on both hind feet (Fig. 11A,
422 dashed curve) agreed with experimental observations (Fig. 11A, solid curve). The slight under-
423 prediction of the oscillation magnitudes of $v_{z,\text{CoM}}$ was likely due to an over-estimation of duty
424 factor on the granular surface. This is because F_z may have dropped to zero even before takeoff if
425 the foot started moving upward before takeoff (Fig. 10).

426 *Mechanical energetics on granular surface*

427 Using the measured CoM kinematics, assumed foot rotation, and calculated vertical ground
428 reaction force, we examined the mechanical energetics of the lizard running on the granular
429 surface (Table 3, Fig. 11D). In the first half of stance, the mechanical energy of the CoM
430 decreased significantly from $E_{\text{touchdown}} = 1.00 \pm 0.00$ at touchdown to $E_{\text{mid-stance}} = 0.86 \pm 0.09$ at
431 mid-stance ($F_{2,18} = 6.6132$, $P = 0.007$, ANOVA, Tukey HSD). In the second half of stance, the
432 mechanical energy of the CoM recovered to $E_{\text{aerial}} = 0.99 \pm 0.10$ at mid aerial phase, not
433 significantly different from $E_{\text{touchdown}}$ (Tukey HSD). The reduction in CoM mechanical energy in

434 the first half of stance $\Delta E_{\text{mech}} = 0.14 \pm 0.09$ is the mechanical work needed per step on the
435 granular surface. By integration of F_z over vertical displacement of the foot during stance (see
436 Appendix), the energy lost to the granular substrate per step was estimated as $E_{\text{substrate}} = 0.17 \pm$
437 0.05 , not significantly different from ΔE_{mech} ($F_{1,12} = 0.4659$, $P = 0.5078$, ANOVA). Note that the
438 energies of each run were normalized to $E_{\text{touchdown}}$ of that run.

439

440

Discussion

441

Conservation of spring-mass-like CoM dynamics on solid and granular surfaces

442 The observed kinematics and calculated mechanical energetics demonstrated that the zebra-tailed
443 lizard ran like a spring-mass system on both solid and granular surfaces. On both surfaces, the
444 CoM forward speed (Fig. 5B), vertical position (Fig. 5C), and lateral position (Fig. 5D) displayed
445 oscillation patterns that are in accord with predictions from the Spring-Loaded Inverted Pendulum
446 (SLIP) model (Blickhan, 1989) and the Lateral Leg Spring (LLS) model (Schmitt et al., 2002).
447 The small relative oscillations of the CoM forward speed (i.e., $\Delta v_{x,\text{CoM}}/v_{x,\text{CoM}} \ll 1$) was expected
448 because the Froude number was large for the lizard (see Appendix). The substantial sprawling of
449 the legs contributed to the medio-lateral oscillatory motion of the animal. Furthermore, on both
450 surfaces, the mechanical energy of the CoM oscillated within a step, reaching minimum at mid-
451 stance and maximum during the aerial phase (Fig. 9F, 11D), a defining feature of spring-mass
452 like running (Blickhan, 1989; Schmitt et al., 2002).

453 To our knowledge, ours is the first study to quantitatively demonstrate spring-mass-like CoM
454 motion in lizards running on granular surfaces. Spring-mass-like CoM motion was previously
455 observed in other lizards and geckos running on solid surfaces (Farley and Ko, 1997; Chen et al.,
456 2006), but it was not clear whether energy-saving by elastic elements played an important role.

457

Hind foot function on solid surface: energy-saving spring

458 Our study is also the first to quantify elastic energy savings in foot tendons in lizards during
459 running on solid surfaces. The significant energy savings (about 40% of the mechanical work
460 needed per step) in the zebra-tailed lizard's hind foot tendons is in a similar range to the energy
461 savings by ankle extensor tendons and digital flexor tendons and ligaments in larger animals
462 (Alexander, 2003), such as kangaroos (50%, Alexander and Vernon, 1975), wallabies (45%,

463 Biewener et al., 1998), horses (40%, Biewener, 1998b), and humans (35%, with an additional 17%
464 from ligaments in the foot arch, Ker et al., 1987).

465 This is surprising considering that the elastic energy saving mechanism was previously thought
466 less important in small animals (e.g., 14% in hopping kangaroo rat of ~ 100 g mass, Biewener et
467 al., 1981). Because the tendons of small animals are “overbuilt” to withstand large stresses during
468 escape, during steady-speed locomotion these tendons usually experience stresses too small to
469 induce significant elastic energy storage and return (Biewener and Blickhan, 1988; McGowan et
470 al., 2008). We verified that for zebra-tailed lizards running at ~ 1 m/s the maximal stress in the
471 foot tendons is 4.3 MPa (see Appendix), well below the 100 MPa breaking stress for most
472 tendons (Kirkendall and Garrett, 1997).

473 The zebra-tailed lizard’s elongate hind foot and digitigrade foot posture on the solid surface may
474 be an adaptation for elastic energy saving during rapid locomotion. Like other iguanids (Russell,
475 1993), this lizard does not have substantial ankle extensor tendons as large animals do.
476 Nevertheless, elongation of foot tendons and a digitigrade posture enhance the hind foot’s energy
477 saving capacity by decreasing tendon stiffness and mechanical advantage (Biewener et al., 2004)
478 (see Appendix). A recent study also found significant energy savings (53%) by elongate foot
479 tendons in running ostriches (Rubenson et al., 2011). More generally, elongation of distal limb
480 segments such as legs, feet, and toes which possess tendons may be an adaptation for energy
481 saving during rapid locomotion. Indeed, many cursorial animals including mammals (Garland Jr.
482 and Janis, 1993), lizards (Bauwens et al., 1995), and dinosaurs (Coombs Jr., 1978) display
483 elongation of distal limb segments. Short fascicles and long tendons and ligaments are often
484 found in the ankle extensor muscles and digital flexor muscles in large cursorial ungulates such as
485 horses, camels, and antelopes (Alexander, 2003).

486 *Solid surface model assumptions*

487 Our estimates of elastic energy storage and return on the solid surface assume isometric
488 contraction of lower leg muscles. However, muscles have a finite stiffness and do lengthen by a
489 small amount under limb tension (Biewener, 1998a; Roberts et al., 1997). Despite this difference,
490 our estimates still hold, because in the latter case both lower leg muscles and foot tendons behave
491 like springs, and the total stiffness remains the same (since external force and total deformation
492 remain the same). In the case where the muscles actively shorten during stance and further
493 lengthen the tendons (which does positive mechanical work on the tendons), the energy storage
494 and return in the tendons would increase. However, the overall energy efficiency would decrease

495 (with everything else being the same), because apart from energy lost in tendon recoil, energy is
496 further lost in the muscles that perform the mechanical work, i.e., muscle work is more expensive
497 than tendon work (Biewener and Roberts, 2000).

498 In addition, the hind limb resilience obtained from anesthetized lizards was assumed to be a good
499 estimate for hind limb resilience in running lizards. This is based on our observations that
500 resilience was independent of torque, angular displacement, and loading rate, as well as previous
501 findings that the damping properties of animal limbs are largely intrinsic to their structure and
502 material properties (Weiss et al., 1988; Fung, 1993; Dudek and Full, 2006). Future studies using
503 techniques such as tendon buckles (Biewener et al., 1998), sonomicrometry (Biewener et al.,
504 1998), ultrasonography (Maganaris and Paul, 1999), and oxygen consumption measurement
505 (Alexander, 2003) during locomotion are needed to confirm this assumption.

506 *Hind foot function on granular surface: dissipative, force-generating paddle*

507 The similarity between the observed and predicted $v_{z,CoM}$ on the granular surface supports the
508 hypothesis of subsurface foot rotation. We speculate that on the granular surface the foot
509 functions as a “paddle” through fluidized grains to generate force. This differs from previous
510 observations of the utilization of solidification forces of the granular media in a legged robot (Li
511 et al., 2009; Li et al., 2010b) and sea turtle hatchlings (Mazouchova et al., 2010) moving on
512 granular surfaces.

513 As the zebra-tailed lizard’s hind foot paddles through fluidized grains to generate force, energy is
514 lost to the substrate because grain contact forces in granular media are dissipative (Nedderman,
515 1992). A large foot can reduce energy loss to the granular substrate compared to a small one,
516 much like large snowshoes used by humans can reduce energy cost for walking on snow (Knapik
517 et al., 1997). From our model of foot-ground interaction on the granular surface, for a given
518 animal (constant weight), energy loss to the substrate is proportional to foot penetration depth,
519 and thus inversely proportional to foot area and substrate strength (see Appendix).

520 *Granular surface model assumptions*

521 In our modeling of the foot-ground interaction on the granular surface using the penetration force
522 model, we made two assumptions. First, we assumed that the ground reaction forces were
523 insensitive to speed. This is true in the low speed regime (<0.5 m/s for our glass particles,
524 Maladen et al., 2009) where particle inertia is negligible and forces are dominated by particle
525 friction. Because friction is proportional to pressure, and pressure is proportional to depth (Hill et

526 al., 2005), granular forces in the low-speed regime are proportional to depth ($F_z = \alpha|z|A$),
527 analogous to the hydrostatic forces in fluids ($F_z = \rho g|z|A$, i.e. buoyant forces due to hydrostatic
528 pressure).

529 Second, we used the vertical stress per unit depth α determined from vertical penetration of a
530 horizontally oriented disc to estimate forces on the foot as it rotates subsurface. In this calculation,
531 the effective vertical stress per unit depth $\alpha \cos\theta_{\text{foot}}$ (see Appendix) depended on foot orientation
532 via a simple relation $\cos\theta_{\text{foot}}$ (because projected area $A = A_{\text{foot}} \cos\theta_{\text{foot}}$; see Appendix), and not on
533 direction of motion. However, our recent physics experiments (Li et al., in preparation) suggest
534 that stresses in granular media in the low speed regime depend on both orientation and direction
535 of motion in a more complicated manner, and that $\alpha \cos\theta_{\text{foot}}$ overestimates vertical stress per unit
536 depth for all foot orientations and directions of motion except when the foot is horizontal and
537 moving vertically downwards. Therefore, our model must be overestimating hydrostatic-like
538 forces, and there must be additional forces contributing to the lizard's ground reaction forces.

539 We propose that these additional forces are likely from hydrodynamic-like inertial forces
540 resulting from the local acceleration of the substrate (particles) by the foot. Analogous to
541 hydrodynamic forces in fluids (Vogel, 1996), for an intruder moving rapidly in granular media,
542 the particles initially at rest in front of the intruder are accelerated by, and thus exert reaction
543 forces on, the intruder. Hydrodynamic-like forces at ~ 1 m/s can play an important role both in
544 impact forces on free falling intruders (Katsuragi and Durian, 2007; Goldman and Umbanhowar,
545 2008) and in legged locomotion of small lightweight robots (Qian et al., 2012). We note that the
546 foot rotation hypothesis should hold regardless, because hydrodynamic-like forces are also
547 proportional to projected area (Katsuragi and Durian, 2007).

548 However, we know too little about the lizard's subsurface foot kinematics and the force laws in
549 the high-speed regime on an intruder being pushed in a complex path within granular media (not
550 simply a free-falling intruder) to more accurately calculate both hydrostatic-like and
551 hydrodynamic-like forces. Future x-ray high-speed imaging experiments (Maladen et al 2009;
552 Sharpe et al., 2012) will reveal how the lizard foot was moving subsurface. Further studies of
553 intrusion forces in granular media in both low-speed (Li et al., 2013) and high-speed regimes can
554 provide a more comprehensive understanding of ground reaction forces during legged locomotion
555 on granular surfaces and provide better estimates of foot penetration depth and energy loss.

556 *Comparison to water-running in basilisk lizard*

557 The rapid impact of the foot on the surface at touchdown and hypothesized subsurface foot
558 rotation appear kinematically similar to the slap and stroke phases of the basilisk lizards running
559 on the surface of water (Glasheen and McMahon, 1996a; Hsieh, 2003). For the zebra-tailed lizard
560 running on sand, both granular hydrostatic-like and hydrodynamic-like forces can contribute to
561 vertical ground reaction force. This is also qualitatively similar to water-running basilisk lizard,
562 which utilizes both hydrostatic forces resulting from the hydrostatic pressure between the water
563 surface and the bottom of the air cavity created by the foot, and hydrodynamic forces resulting
564 from the water being accelerated from rest by the rapidly moving foot (Glasheen and McMahon,
565 1996a, 1996b; Hsieh and Lauder, 2004).

566 However, the degree to which each species relies on these two categories of forces differs due to
567 differences in the properties of the supporting media. For given foot size, depth, and speed, the
568 hydrostatic(-like) forces in water are an order of magnitude smaller than the hydrostatic-like
569 forces in granular media, whereas the hydrodynamic(-like) forces are similar between in water
570 and in granular media (see Appendix). As a result, the basilisk lizard running on water must rely
571 on hydrodynamic forces to a larger degree than the zebra-tailed lizard running on sand,
572 considering that these two lizards have similar size (~ 0.1 m). An extreme example for this is that
573 it is impossible for a basilisk lizard to stand on the surface of water, but a zebra-tailed lizard can
574 stand on loose sand.

575 *Motor function of upper hind leg*

576 Despite the passive nature of the leg spring in the spring-mass model, animal limbs do not
577 function purely passively as springs—the muscles within them must perform mechanical work.
578 We have shown that on the solid surface, the lizard’s hind foot saves about 40% of the
579 mechanical work per step. The remaining 60% is lost either within the foot or to the ground, and
580 must be compensated by mechanical work performed by muscles, which is $W_{\text{muscle}} = 0.11 \pm 0.10$.
581 This work is likely provided by knee extension during the second half of stance (Fig. 6D, red
582 curve) powered by the upper leg muscles.

583 On the granular surface, substantial energy is lost to the substrate. This is in accord with previous
584 observations of higher mechanical energetic cost during locomotion on granular surfaces in
585 human (Zamparo et al., 1992; Lejeune et al., 1998) and legged robots (Li et al., 2010a). Because
586 the energy lost to the substrate equals the reduction in CoM mechanical energy during the first
587 half of stance, even without energy loss within the limb, the upper hind leg muscles must perform
588 mechanical work of $W_{\text{muscle}} = 0.31 \pm 0.10$ during the second half of stance, about three times that

589 on the solid surface for a given animal running at a given speed, as evidenced by the larger knee
590 extension on the granular surface (Fig. 6D, blue curve).

591 Our models of the foot-ground interaction on both surfaces assume purely passive foot mechanics,
592 and do not consider the role of active neurosensory control. However, animals can actively adjust
593 kinematics and muscle function to accommodate changes in surface conditions (Ferris et al., 1999;
594 Daley and Biewener, 2006). We observed that when confronted by a substrate which transitioned
595 from solid into granular (or *vice versa*), the lizard displayed partial adjustment of foot posture
596 during the first step on the new surface, followed by full adjustment during the second step.
597 Future studies using neuromechanics techniques, such as EMG (Biewener et al., 1998; Sponberg
598 and Full, 2008; Sharpe and Goldman, in review) and denervation and reinnervation (Chang et al.,
599 2009), can determine how neural control and sensory feedback mechanisms are used to control
600 limb function to accommodate changing substrates.

601 *Conclusions*

602 During running on both solid and granular surfaces, the zebra-tailed lizard displayed spring-mass-
603 like center of mass kinematics with distinct hind foot, hind leg, and trunk kinematics. The lizard's
604 large, elongate hind foot served multiple functions during locomotion. On the solid surface, the
605 hind foot functioned as an energy-saving spring and reduced about 40% of the mechanical work
606 needed each footstep. On the granular surface, the hind foot paddled through fluidized grains to
607 generate force, and substantial energy was lost during irreversible deformation of the granular
608 substrate. The energy lost within the foot and to the substrate must be compensated for by
609 mechanical work done by the upper hind leg muscles.

610 The multifunctional hind foot may passively (and possibly actively) adjust to the substrate during
611 locomotion in natural terrain, and provide this desert generalist with energetic advantages and
612 simplify its neurosensory control tasks (Full and Koditschek, 1999). Current robotic devices often
613 suffer performance loss and high cost of transport on flowing substrates like granular material
614 (Kumagai 2004; Li et al., 2009; Li et al., 2010b; Li et al., 2010a). Insights from studies like ours
615 can provide inspiration for next-generation multi-terrain robots (Pfeifer et al., 2007). Finally, our
616 study also highlights the need for comprehensive force models for granular media (Li et al., in
617 preparation) and for flowing terrestrial environments in general.

618

619 **Appendix**

620

Small relative oscillation in forward speed

621 Running at 1.1 m/s, the lizard's Froude number in the sagittal plane was $Fr = v_{x,CoM}^2/gL_0 = 3$
622 (where $L_0 \approx 4$ cm is the leg length at touchdown), above the typical value of 2.5 where most
623 animals transition from trotting to galloping (Alexander, 2003). This implied that the kinetic
624 energy ($\frac{1}{2} m v_{CoM}^2 \approx \frac{1}{2} m v_{x,CoM}^2$) of the CoM was 3 times larger than its gravitational potential
625 energy (mgz_{CoM}). Because both the forward speed oscillation $\Delta v_{x,CoM}$ and vertical speed oscillation
626 $\Delta v_{z,CoM}$ were determined by the total ground reaction force and the attack angle of the leg spring
627 ($\beta = \sin^{-1}(v_{x,CoM}DT/2L_0) = 0.9$ rad), they must be of the same order of magnitude (Blickhan, 1989),
628 i.e., $\Delta v_{x,CoM} \sim \Delta v_{z,CoM}$. From the observed CoM kinematics, $\Delta v_{z,CoM} < (gL_0)^{1/2}$. Therefore, $\Delta v_{x,CoM} \sim$
629 $\Delta v_{z,CoM} < (gL_0)^{1/2} \ll v_{x,CoM}$, and $\Delta v_{x,CoM}/v_{x,CoM} \ll 1$.

630

Hind foot curvature on solid surface

631 Three-dimensional kinematics showed that the hind limb (from the hip to the digit tip of the
632 fourth toe) remained nearly within a plane during the entire stride (out-of-plane component is 5%
633 averaged over the entire stride). During stance, the orientation of the foot plane remained nearly
634 unchanged, with a foot sprawl angle of $53 \pm 4^\circ$ relative to the sagittal plane in the posterior view.
635 Hind foot curvature κ could then be obtained by fitting a circle to the hind foot (from the ankle to
636 the digit tip) within the foot plane and determining the radius of curvature ρ of the fit circle (see
637 diagram in Fig. 9A), i.e., $\kappa = \pm 1/\rho$, where + sign indicates foot hyperextension, – sign indicates
638 foot flexion, and $\kappa = 0$ indicates a straight foot.

639

Tendon spring deformation

640 From the two-dimensional strut-spring model of the hind limb, by geometry, the tendon spring
641 deformation Δl was related to the observed changes of joint angles and the foot joint radii as: $\Delta l =$
642 $\sum_i r_i \Delta \theta_i$, where $i = K, A, MP, PP$ were the four joints in the model, $\Delta \theta_i$ the observed changes of
643 joint angles, and r_i the joint radii ($r_K = r_A = 1.25$ mm, $r_{MP} = 0.75$ mm, $r_{PP} = 0.50$ mm). We
644 observed that the relaxed hind foot of a live animal was nearly straight (Fig. 1A), which was
645 similar to the foot shape at touchdown during running (Fig. 3A,E). Thus we defined the relaxed
646 length of the tendon spring as the length when the foot was straight, i.e., $\Delta l = 0$ at touchdown.
647 Calculated maximal tendon spring deformation $\Delta l_{max} = 0.78$ mm corresponded to a 3% strain. We
648 did not consider tendon spring deformation in the swing phase (dotted curve in Fig. 6F) because
649 the assumption of isometric contraction of lower leg muscles was only valid for the stance phase.

650

Tendon spring stiffness

651 The stiffness of the tendon spring was defined as the maximal tension divided by the maximal
652 deformation of the tendon spring, i.e., $k = T_{\max}/\Delta l_{\max}$. From the observed CoM kinematics, the
653 total ground reaction force at mid-stance was $F_{\max} = 0.3$ N within the coronal plane and pointed
654 from the digit tip to the hip. At mid-stance, because the foot was neither dorsiflexing nor
655 plantarflexing, torque was balanced at the ankle, i.e., $T_{\max}r_A = F_{\max}\Delta x_{AT}$, where $\Delta x_{AT} = 1.4$ cm was
656 the horizontal distance between the ankle and the digit tip at mid-stance, and $r_A = 1.25$ mm. Thus
657 $T_{\max} = 3.4$ N and $k = 4.4 \times 10^3$ N/m. The maximal stress in the foot tendons during stance was
658 $\sigma_{\max} = T_{\max}/\pi r_{pp}^2 = 4.3$ MPa.

659 The torsional stiffness of the ankle observed in anesthetized lizards from the modified work loop
660 experiments ($\sim 1 \times 10^{-3}$ Nm/rad) was an order of magnitude smaller than estimated from running
661 kinematics (12×10^{-3} Nm/rad). This is however not contradictory but expected because during
662 stance the lizard's lower leg muscles must be activated, and the resulting higher tension from
663 muscle contraction increases limb stiffness (Weiss et al., 1988).

664

Foot elongation increases energy savings on solid surface

665 The stiffness of a piece of elastic material like a tendon is $k = E_0A_0/l_0$, where E_0 is the Young's
666 modulus, A_0 the cross sectional area, and l_0 the rest length of the material. Most animal tendons
667 are primarily made of collagen (Kirkendall and Garrett, 1997) and are of similar Young's
668 modulus (i.e., E_0 is nearly constant). Thus, the stiffness of the tendon spring scales as $k \propto A_0/l_0 \propto$
669 r_0^2/l_0 , i.e., an elongate tendon (smaller r_0 and larger l_0) is less stiff and stretches more easily than
670 a short, thick tendon. Because elastic energy storage decreases with tendon stiffness ($E_{\text{storage}} = \frac{1}{2}$
671 $k\Delta l_{\max}^2 = \frac{1}{2} T_{\max}^2/k \propto 1/k$ for a given T_{\max}), an elongate tendon can store (and return) more energy.

672 An elongate foot also reduces the moment arm of tendon tension (small r_A) but increases the
673 moment arm of the ground reaction force (large Δx_{AT}) about the ankle, therefore reducing the
674 mechanical advantage (Biewener et al., 2004), so it increases tension in the foot for a given
675 ground reaction force (because $T_{\max} = F_{\max}\Delta x_{AT}/r_A$) and amplifies tendon stretch for enhanced
676 energy storage and return.

677

Vertical ground reaction force on granular surface

678 We assumed that the hind foot was rotating at a constant angular velocity ω about the moving
679 ankle during stance, i.e., $\theta_{\text{foot}} = \omega t$ within $0 \leq t \leq DT$ and $0 \leq \theta_{\text{foot}} \leq \pi/2$, then $\omega = \pi/2DT = 10\pi/9T$

680 = 35 rad/s. From the measured vertical speed of the ankle and this assumed foot rotation, the
 681 vertical speed of most (75%) of the foot was always below 0.5 m/s during most (75%) of stance.

682 Given foot rotation $\theta_{\text{foot}} = \omega t$, the foot area projected in the horizontal plane decreased with time
 683 as $A = A_{\text{foot}} \cos \omega t$, where $A_{\text{foot}} = 1 \text{ cm}^2$ is the hind foot area; the foot depth (measured at the center
 684 of the foot) increased with time as $|z| = |z|_{\text{max}} \sin \omega t$. The vertical ground reaction force on the foot
 685 was then sinusoidal: $F_z = F_{z,\text{max}} \sin 2\omega t$, which was sinusoidal, where $F_{z,\text{max}} =$
 686 $\alpha A_{\text{foot}} / |z|_{\text{max}} \sin \pi / 4 \cos \pi / 4 = \frac{1}{2} \alpha A_{\text{foot}} / |z|_{\text{max}}$. For steady state locomotion on a level surface, the F_z
 687 generated by one foot averaged over a cycle must equal half the body weight, i.e.,
 688 $\int_0^T F_{z,\text{max}} \sin 2\omega t dt = \frac{1}{2} mg$. Therefore, $F_{z,\text{max}} = 5\pi mg / 9$ and $F_z = 5\pi mg / 9 \sin 10\pi t / 9T$.

689 *Energy loss to granular substrate*

690 By integration of vertical ground reaction force over vertical displacement of the foot, the energy
 691 loss to the granular substrate was $E_{\text{substrate}} = \int_0^{|z|_{\text{max}}} F_z d|z| = \int_0^T F_z \frac{d|z|}{dt} dt$, where $|z|_{\text{max}} = 1.0 \text{ cm}$
 692 from $F_{z,\text{max}} = \frac{1}{2} \alpha A_{\text{foot}} / |z|_{\text{max}}$. The hypothesized foot rotation in the sagittal plane did not take into
 693 account the sprawl of the foot during stance, which could induce additional energy loss by lateral
 694 displacement of the granular substrate. However, a sprawled foot posture did not affect the
 695 condition of vertical force balance and thus did not change our estimate of energy dissipation in
 696 the sagittal plane. Therefore this estimate provides a lower bound.

697 *Large foot area reduces energy loss on granular surface*

698 For a given animal (constant weight mg), $F_{z,\text{max}} = \frac{1}{2} \alpha A_{\text{foot}} / |z|_{\text{max}} = 5\pi mg / 9$ is constant, thus $E_{\text{substrate}}$
 699 $= |z|_{\text{max}} \int_0^T F_z \omega \cos \omega t dt \propto |z|_{\text{max}} \propto 1 / (\alpha A_{\text{foot}})$. This implies that the energy loss to the granular
 700 substrate increases with foot penetration depth. On a given granular surface (fixed α), a larger
 701 foot (larger A_{foot}) sinks less than a smaller foot, and thus loses less energy to the substrate. For a
 702 given foot size (fixed A_{foot}), a foot sinks less on a stronger granular substrate (larger α) than on a
 703 weaker substrate, and thus loses less energy to the substrate.

704 *Comparison of forces in granular media and in water*

705 For water, hydrostatic force is $F_z = \rho g |z| A$. Comparing this with $F_z = \alpha |z| A$ for granular media, ρg
 706 is the equivalent of α . For water, $\rho g = 1.0 \times 10^4 \text{ N/m}^3$; for loosely packed glass particles, $\alpha = 3.5$
 707 $\times 10^5 \text{ N/m}^3$. Therefore, the hydrostatic forces in water are an order of magnitude smaller than the
 708 hydrostatic-like forces in granular media for given foot size and depth.

709 Hydrodynamic(-like) forces should be proportional to the density of the surrounding media
710 because they are due to the media being accelerated. For water, $\rho = 1.0 \times 10^3 \text{ N/m}^3$; for loosely
711 packed glass particles the effective density is $2.5 \times 10^3 \text{ N/m}^3 \times 0.58 \text{ volume fraction} = 1.45 \times 10^3$
712 N/m^3 . Therefore, the hydrodynamic forces in water and hydrodynamic-like forces in granular
713 media are on the same order of magnitude for given foot size and foot speed.

714

715

Acknowledgements

716 We gratefully thank Sarah Sharpe, Yang Ding, Nick Gravish, Ryan Maladen, Paul Umbanhowar,
717 Kyle Mara, Young-Hui Chang, Andy Biewener, Tom Roberts, Craig McGowan, and two
718 anonymous reviewers for helpful discussions and/or comments on the manuscript; Loretta Lau for
719 help with kinematics data tracking; Sarah Sharpe for help with animal protocol and
720 anesthetization; Mateo Garcia, Nick Gravish, and Andrei Savu for help with force plate setup;
721 Ryan Maladen and The Sweeney Granite Mountains Desert Research Center for help with animal
722 collection; and the staff of The Physiological Research Laboratory animal facility of The Georgia
723 Institute of Technology for animal housing and care. This work was funded by The Burroughs
724 Wellcome Fund (D.I.G. and C.L.), The Army Research Laboratory Micro Autonomous Systems
725 and Technology Collaborative Technology Alliance (D.I.G. and C.L.), The Army Research
726 Office Biological Locomotion Principles and Rheological Interaction Physics (D.I.G. and C.L.)
727 and The University of Florida and Temple University start-up funds (S.T.H.).

728

729

References

730 **Alexander, R. M.** (2003). *Principles of Animal Locomotion*. Princeton: Princeton University
731 Press.

732 **Alexander, R. M. and Vernon, A.** (1975). The mechanics of hopping by kangaroos
733 (*Macropodidae*). *Journal of Zoology* **177**, 265–303.

734 **Autumn, K., Liang, Y. A., Hsieh, S. T., Zesch, W., Chan, W. P., Kenny, T. W., Fearing, R. S.**
735 **and Full, R. J.** (2000). Adhesive force of a single gecko foot-hair. *Nature* **405**, 681–685.

- 736 **Bauwens, D., Garland Jr., T., Castilla, A. M. and Van Damme, R.** (1995). Evolution of sprint
737 speed in lacertid lizards: morphological, physiological and behavioral covariation. *Evolution* **49**,
738 848–863.
- 739 **Biewener, A. A.** (1998a). Muscle function in vivo: A comparison of muscles used for elastic
740 energy savings versus muscles used to generate mechanical power. *Integrative & Comparative*
741 *Biology* **38**, 703–717.
- 742 **Biewener, A. A.** (1998b). Muscle-tendon stresses and elastic energy storage during locomotion in
743 the horse. *Comparative Biochemistry and Physiology Part B: Biochemistry & Molecular Biology*
744 **120**, 73–87.
- 745 **Biewener, A. A., Alexander, R. M. and Heglund, N. C.** (1981). Elastic energy storage in the
746 hopping of kangaroo rats (*Dipodomys spectabilis*). *Journal of Zoology* **195**, 369–383.
- 747 **Biewener, A. A. and Blickhan, R.** (1988). Kangaroo rat locomotion: design for elastic energy
748 storage or acceleration? *The Journal of Experimental Biology* **140**, 243–255.
- 749 **Biewener, A. A., Farley, C. T., Roberts, T. J. and Tomaner, M.** (2004). Muscle mechanical
750 advantage of human walking and running: implications for energy cost. *Journal of Applied*
751 *Physiology* **97**, 2266–2274.
- 752 **Biewener, A. A., Konieczynski, D. D. and Baudinette, R. V.** (1998). In vivo muscle force-
753 length behavior during steady-speed hopping in tammar wallabies. *The Journal of Experimental*
754 *Biology* **201**, 1681–1694.
- 755 **Biewener, A. A. and Roberts, T. J.** (2000). Muscle and tendon contributions to force, work, and
756 elastic energy savings: a comparative perspective. *Exercise and Sport Sciences Reviews* **28**, 99–
757 107.
- 758 **Blickhan, R.** (1989). The spring-mass model for running and hopping. *Journal of Biomechanics*
759 **22**, 1217–1227.
- 760 **Blickhan, R. and Full R. J.** (1993). Similarity in multilegged locomotion: Bouncing like a
761 monopode. *Journal of Comparative Physiology* **173**, 509–517.
- 762 **Chang, Y.-H., Auyang, A. G., Scholz, J. P. and Nichols, T. R.** (2009). Whole limb kinematics
763 are preferentially conserved over individual joint kinematics after peripheral nerve injury. *The*
764 *Journal of Experimental Biology* **212**, 3511–3521.

- 765 **Chen, J. J., Peattie, A. M., Autumn, K. and Full, R. J.** (2006). Differential leg function in a
766 sprawled-posture quadrupedal trotter. *The Journal of Experimental Biology* **209**, 249–259.
- 767 **Coombs Jr., W. P.** (1978). Theoretical aspects of cursorial adaptations in dinosaurs. *The*
768 *Quarterly Review of Biology* **53**, 393–418.
- 769 **Crawford, C. S.** (1981). *Biology of Desert Invertebrates*. New York: Springer.
- 770 **Daley, M. A. and Biewener, A. A.** (2006). Running over rough terrain reveals limb control for
771 intrinsic stability. *Proceedings of the National Academy of Sciences of the United States of*
772 *America* **103**, 15681–15686.
- 773 **Dickinson, M. H., Farley, C. T., Full, R. J., Koehl, M. A. R., Kram, R. and Lehman, S.**
774 (2000). How animals move: An integrative view. *Science* **288**, 100–106.
- 775 **Dickinson, W. W. and Ward, J. D.** (1994). Low depositional porosity in eolian sands and
776 sandstones, Namib Desert. *Journal of Sedimentary Research* **64**, 226–232.
- 777 **Ding, Y., Gravish, N. and Goldman, D. I.** (2011a). Drag induced lift in granular media.
778 *Physical Review Letters* **106**, 028001(1–4).
- 779 **Dudek, D. M. and Full, R. J.** (2006). Passive mechanical properties of legs from running insects.
780 *The Journal of Experimental Biology* **209**, 1502–1515.
- 781 **Farley, C. T. and Ko, T. C.** (1997). Mechanics of locomotion in lizards. *The Journal of*
782 *Experimental Biology* **200**, 2177–2188.
- 783 **Ferris, D., Liang, K. and Farley, C. T.** (1999). Runners adjust leg stiffness for their first step on
784 a new running surface. *Journal of Biomechanics* **32**, 787–794.
- 785 **Ferris, D. P., Louie, M. and Farley, C. T.** (1998). Running in the real world: Adjusting leg
786 stiffness for different surfaces. *Proceedings of the Royal Society B: Biological Sciences* **265**, 989–
787 994.
- 788 **Full, R. J. and Koditschek, D. E.** (1999). Templates and anchors: neuromechanical hypotheses
789 of legged locomotion on land. *The Journal of Experimental Biology* **202**, 3325–3332.
- 790 **Fung, Y. C.** (1993). *Biomechanics: Mechanical Properties of Living Tissues*. New York:
791 Springer.

- 792 **Garland Jr., T. and Janis, C.** (1993). Does metatarsal/femur ratio predict maximal running
793 speed in cursorial mammals? *Journal of Zoology* **229**, 133–151.
- 794 **Glasheen, J. W. and McMahon, T. A.** (1996a). A hydrodynamic model of locomotion in the
795 Basilisk Lizard. *Nature* **380**, 340–341.
- 796 **Glasheen, J. W. and McMahon, T. A.** (1996b). Vertical water entry of disks at low Froude
797 numbers. *Physics of Fluids* **8**, 2078–2083.
- 798 **Goldman, D. I. and Umbanhowar, P. B.** (2008). Scaling and dynamics of sphere and disk
799 impact into granular media. *Physical Review E* **77**, 021308(1–14).
- 800 **Gravish, N., Umbanhowar, P. B. and Goldman, D. I.** (2010). Force and flow transition in
801 plowed granular media. *Physical Review Letters* **105**, 208301(1–4).
- 802 **Hedrick, T. L.** (2008). Software techniques for two- and three-dimensional kinematic
803 measurements of biological and biomimetic systems. *Bioinspiration & Biomimetics* **3**, 034001(1–
804 6).
- 805 **Hill, G., Yeung, S. and Koehler, S. A.** (2005). Scaling vertical drag forces in granular media.
806 *Europhysics Letters* **72**, 137–143.
- 807 **Holmes, P., Full, R. J., Koditschek, D. and Guckenheimer, J.** (2006). The dynamics of legged
808 locomotion: Models, analyses, and challenges. *SIAM Review* **48**, 207–304.
- 809 **Hsieh, S. T.** (2003). Three-dimensional hindlimb kinematics of water running in the plumed
810 basilisk lizard (*Basiliscus plumifrons*). *The Journal of Experimental Biology* **206**, 4363–4377.
- 811 **Hsieh, S. T. and Lauder, G. V.** (2004). Running on water: Three-dimensional force generation
812 by basilisk lizards. *Proceedings of the National Academy of Sciences of the United States of*
813 *America* **101**, 16784–16788.
- 814 **Irschick, D. J. and Jayne, B. C.** (1999a). Comparative three-dimensional kinematics of the
815 hindlimb for high speed bipedal and quadrupedal locomotion of lizards. *The Journal of*
816 *Experimental Biology* **202**, 1047–1065.
- 817 **Irschick, D. J. and Jayne, B. C.** (1999b). A field study of the effects of incline on the escape
818 locomotion of a bipedal lizard, *Callisaurus draconoides*. *Physiological and Biochemical Zoology*
819 **72**, 44–56.

Li et al. (2012), *The Journal of Experimental Biology*, **215**, 3293–3308. doi:10.1242/jeb.061937

820 **Jindrich, D. L. and Full, R. J.** (1999). Many-legged maneuverability: dynamics of turning in
821 hexapods. *The Journal of Experimental Biology* **202**, 1603–1623.

822 **Karasov, W. H. and Anderson, R. A.** (1998). Correlates of average daily metabolism of field-
823 active zebra-tailed lizards (*Callisaurus draconoides*). *Physiological Zoology* **71**, 93–105.

824 **Katsuragi, H. and Durian, D. J.** (2007). Unified force law for granular impact cratering. *Nature*
825 *Physics* **3**, 420–423.

826 **Ker, R. F., Bennett, M. B., Bibby, S. R., Kester, R. C. and Alexander, R. M.** (1987). The
827 spring in the arch of the human foot. *Nature* **325**, 147–149.

828 **Kirkendall, D. T. and Garrett, W. E.** (1997). Function and biomechanics of tendons.
829 *Scandinavian Journal of Medicine & Science in Sports* **7**, 62–66.

830 **Knapik, J., Hickey, C., Ortega, S., Nagel, J. and De Pontbriand, R.** (2002). Energy cost
831 during locomotion across snow: a comparison of four types of snowshoes with snowshoe design
832 considerations. *Work* **18**, 171–177.

833 **Korff, W. L. and McHenry, M. J.** (2011). Environmental differences in substrate mechanics do
834 not affect sprinting performance in sand lizards (*Uma scoparia* and *Callisaurus draconoides*).
835 *The Journal of Experimental Biology* **214**, 122–130.

836 **Kumagai, J.** (2004). Sand trip—DARPA’s 320-kilometer robotic race across the Mojave Desert
837 yields no winner, but plenty of new ideas. *IEEE Spectrum* **41**, 44–50.

838 **Lejeune, T. M., Willems, P. A. and Heglund, N. C.** (1998). Mechanics and energetics of human
839 locomotion on sand. *The Journal of Experimental Biology* **201**, 2071–2080.

840 **Li, C., Hoover, A. M., Birkmeyer, P., Umbanhowar, P. B., Fearing, R. S. and Goldman, D. I.**
841 (2010a). Systematic study of the performance of small robots on controlled laboratory substrates.
842 *Proceedings of SPIE* **7679**, 76790Z(1–13).

843 **Li, C., Umbanhowar, P. B., Komsuoglu, H. and Goldman, D. I.** (2010b). The effect of limb
844 kinematics on the speed of a legged robot on granular media. *Experimental Mechanics* **50**, 1383–
845 1393.

Li et al. (2012), *The Journal of Experimental Biology*, **215**, 3293–3308. doi:10.1242/jeb.061937

846 **Li, C., Umbanhowar, P. B., Komsuoglu, H., Koditschek, D. E. and Goldman, D. I.** (2009).
847 Sensitive dependence of the motion of a legged robot on granular media. *Proceedings of the*
848 *National Academy of Sciences of the United States of America* **106**, 3029–3034.

849 **Li, C., Zhang, T. and Goldman, D. I.** (2013). A terradynamics of legged locomotion on
850 granular media. *Science*, **339**, 1408–1411.

851 **Maganaris, C. N. and Paul, J. P.** (1999). In vivo human tendon mechanical properties. *Journal*
852 *of Physiology* **521**, 307–313.

853 **Maladen, R. D., Ding, Y., Li, C. and Goldman, D. I.** (2009). Undulatory swimming in sand:
854 Subsurface locomotion of the sandfish lizard. *Science* **325**, 314–318.

855 **Maladen, R. D., Ding, Y., Umbanhowar, P. B., Kamor, A. and Goldman, D. I.** (2011).
856 Mechanical models of sandfish locomotion reveal principles of high performance subsurface
857 sand-swimming. *Journal of The Royal Society Interface* **8**, 1332-1345.

858 **Matson J.** (2010). Unfree Spirit: NASA's Mars rover appears stuck for good. *Scientific American*,
859 **302**, 16.

860 **Mazouchova, N., Gravish, N., Savu, A. and Goldman, D. I.** (2010). Utilization of granular
861 solidification during terrestrial locomotion of hatchling sea turtles. *Biology letters* **6**, 398–401.

862 **McGowan, C. P., Skinner, J. and Biewener, A. A.** (2008). Hind limb scaling of kangaroos and
863 wallabies (superfamily *Macropodoidea*): Implications for hopping performance, safety factor and
864 elastic savings. *Journal of Anatomy* **212**, 153–163.

865 **Moritz, C. T. and Farley, C. T.** (2003). Human hopping on damped surfaces: Strategies for
866 adjusting leg mechanics. *Proceedings of the Royal Society B: Biological Sciences* **270**, 1741–
867 1746.

868 **Mosauer, W.** (1932). Adaptive convergence in the sand reptiles of the Sahara and of California:
869 A study in structure and behavior. *Copeia* **1932**, 72–78.

870 **Nedderman, R. M.** (1992). *Statics and Kinematics of Granular Materials*. Cambridge:
871 Cambridge University Press.

872 **Pfeifer, R., Lungarella, M. and Iida, F.** (2007). Self-organization, embodiment, and
873 biologically inspired robotics. *Science* **318**, 1088–1093.

Li et al. (2012), *The Journal of Experimental Biology*, **215**, 3293–3308. doi:10.1242/jeb.061937

874 **Qian F., Zhang T., Li C., Masarati, P., Hoover A.M., Birkmeyer P., Pullin A., Fearing R.S.**
875 **and Goldman D.I.** (2012). Walking and running on yielding and fluidizing ground. *Robotics:*
876 *Science and Systems* (in press).

877 **Roberts, T. J., Marsh, R. L., Weyand, P. G. and Taylor, C. R.** (1997). Muscular force in
878 running turkeys: The economy of minimizing work. *Science* **275**, 1113–1115.

879 **Rubenson, J., Lloyd, D. G., Heliam, D. B., Besier, T. F. and Fournier, P. A.** (2011).
880 Adaptations for economical bipedal running: The effect of limb structure on three-dimensional
881 joint mechanics. *Journal of The Royal Society Interface* **8**, 740–755.

882 **Russell, A. P.** (1993). The aponeuroses of the lacertilian ankle. *Journal of Morphology* **218**, 65–
883 84.

884 **Schmitt, J., Garcia, M., Razo, R. C., Holmes, P. and Full, R. J.** (2002). Dynamics and stability
885 of legged locomotion in the horizontal plane: A test case using insects. *Biological Cybernetics* **86**,
886 343–353.

887 **Sharpe, S. S., Ding, Y., and Goldman, D. I.** (2012). Environmental interaction influences
888 muscle activation strategy during sand-swimming in the sandfish lizard (*Scincus scincus*). *The*
889 *Journal of Experimental Biology* **216**, 260–274.

890 **Spagna, J. C., Goldman, D. I., Lin, P.-C., Koditschek, D. E. and Full, R. J.** (2007).
891 Distributed mechanical feedback in arthropods and robots simplifies control of rapid running on
892 challenging terrain. *Bioinspiration & Biomimetics* **2**, 9–18.

893 **Spence, A. J., Revzen, S., Seipel, J., Mullens, C. and Full, R. J.** (2010). Insects running on
894 elastic surfaces. *The Journal of Experimental Biology* **213**, 1907–1920.

895 **Sponberg, S. and Full, R. J.** (2008). Neuromechanical response of musculo-skeletal structures in
896 cockroaches during rapid running on rough terrain. *The Journal of Experimental Biology* **211**,
897 433–446.

898 **Vitt, L. J. and Ohmart, R. D.** (1977). Ecology and reproduction of lower Colorado River lizards:
899 I. *Callisaurus draconoides* (Iguanidae). *Herpetologica* **33**, 214–222.

900 **Vogel, S.** (1996). *Life in Moving Fluids: The Physical Biology of Flow*. Princeton: Princeton
901 University Press.

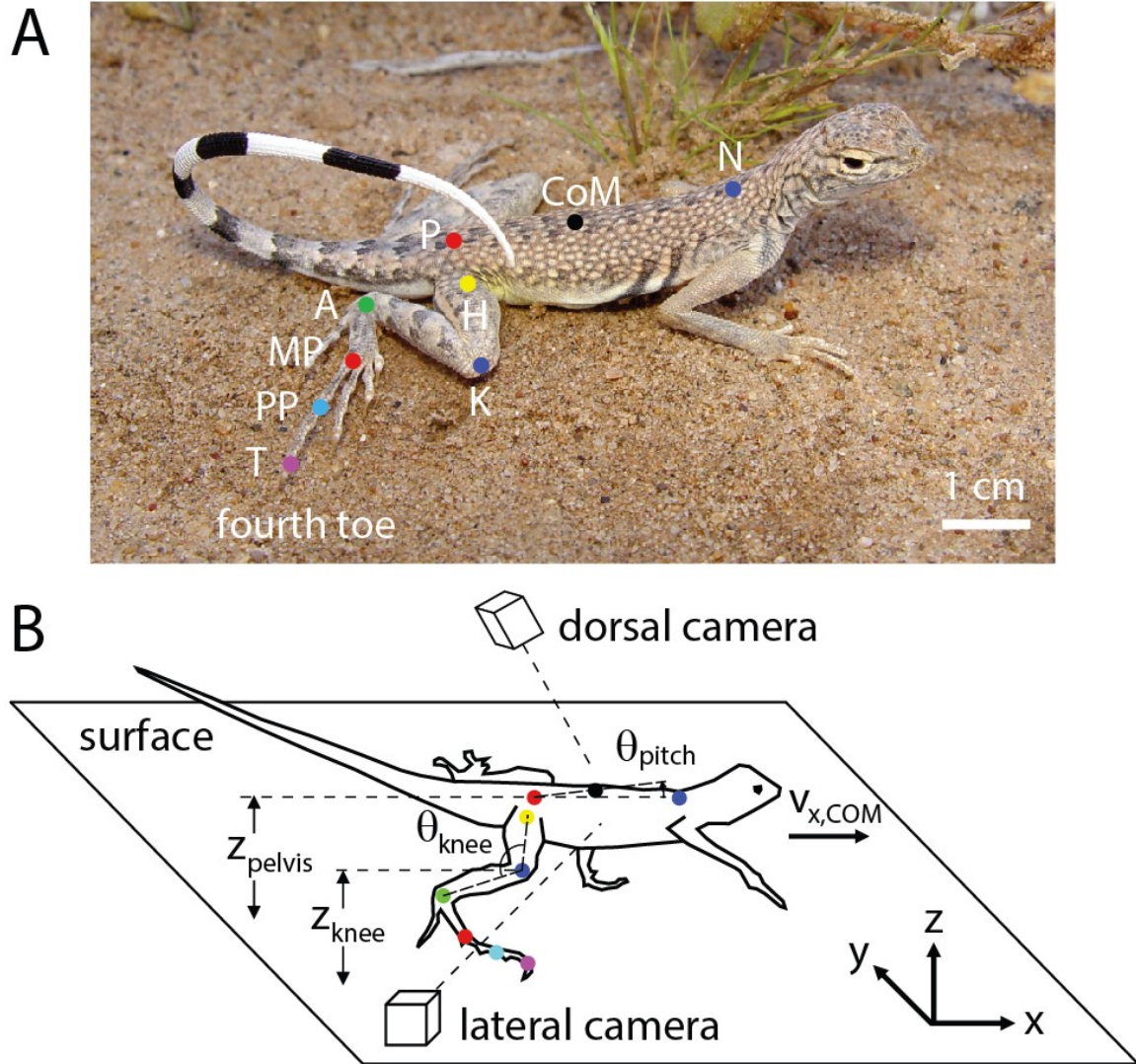
Li et al. (2012), *The Journal of Experimental Biology*, **215**, 3293–3308. doi:10.1242/jeb.061937

902 **Weiss, P. L., Hunter, I. W. and Kearney, R. E.** (1988). Human ankle joint stiffness over the
903 full range of muscle activation levels. *Journal of Biomechanics* **21**, 539–544.

904 **Zamparo, P., Perini, R., Orizio, C., Sacher, M. and Ferretti, G.** (1992). The energy cost of
905 walking or running on sand. *European Journal of Applied Physiology and Occupational*
906 *Physiology* **65**, 183–187.

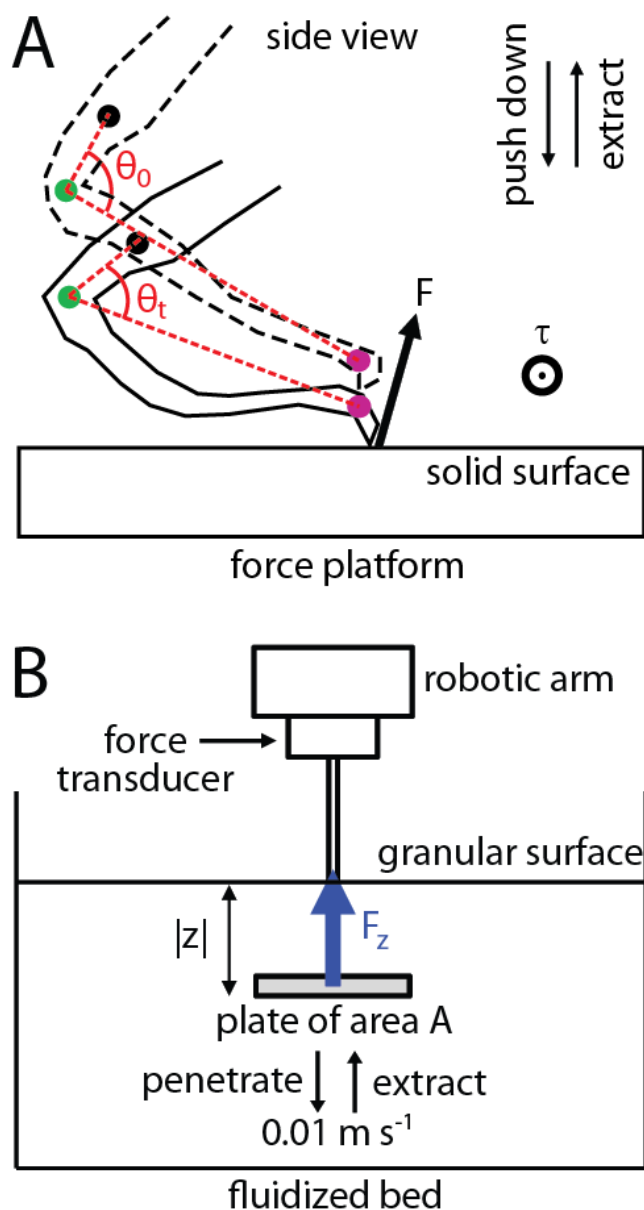
907

908



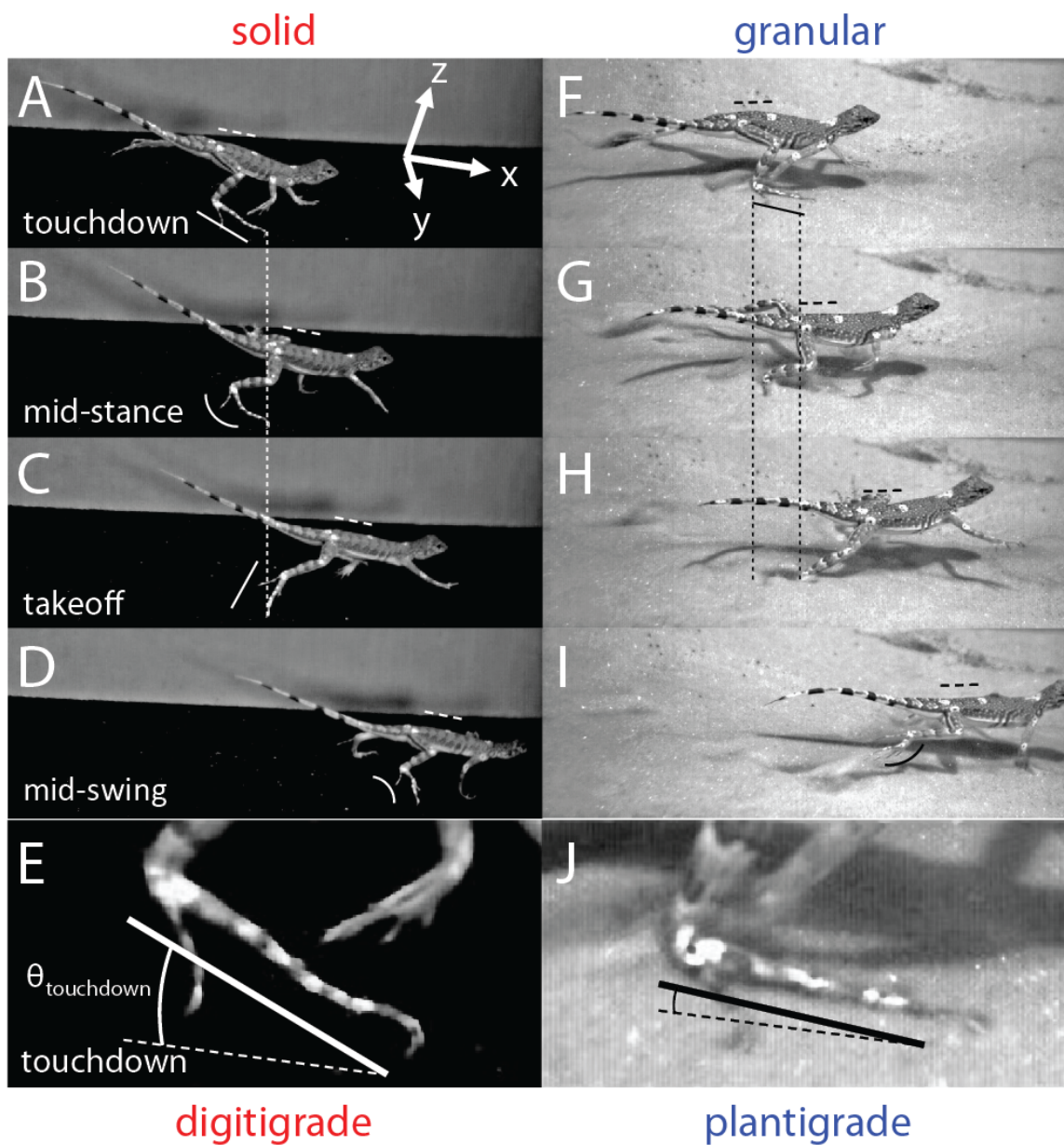
909

910 Fig. 1. Model organism and three-dimensional kinematics experiments. (A) A zebra-tailed lizard
911 resting on sand in the wild (photo: Thomas C. Brennan). (B) Experimental setup for three-
912 dimensional kinematics capture, with definitions of pelvis height (z_{pelvis}), knee height (z_{knee}), trunk
913 pitch angle (θ_{pitch}), and knee angle (θ_{knee}). Colored dots in (A,B) are digitized points on the
914 midline of the trunk, hind leg, and elongate hind foot.



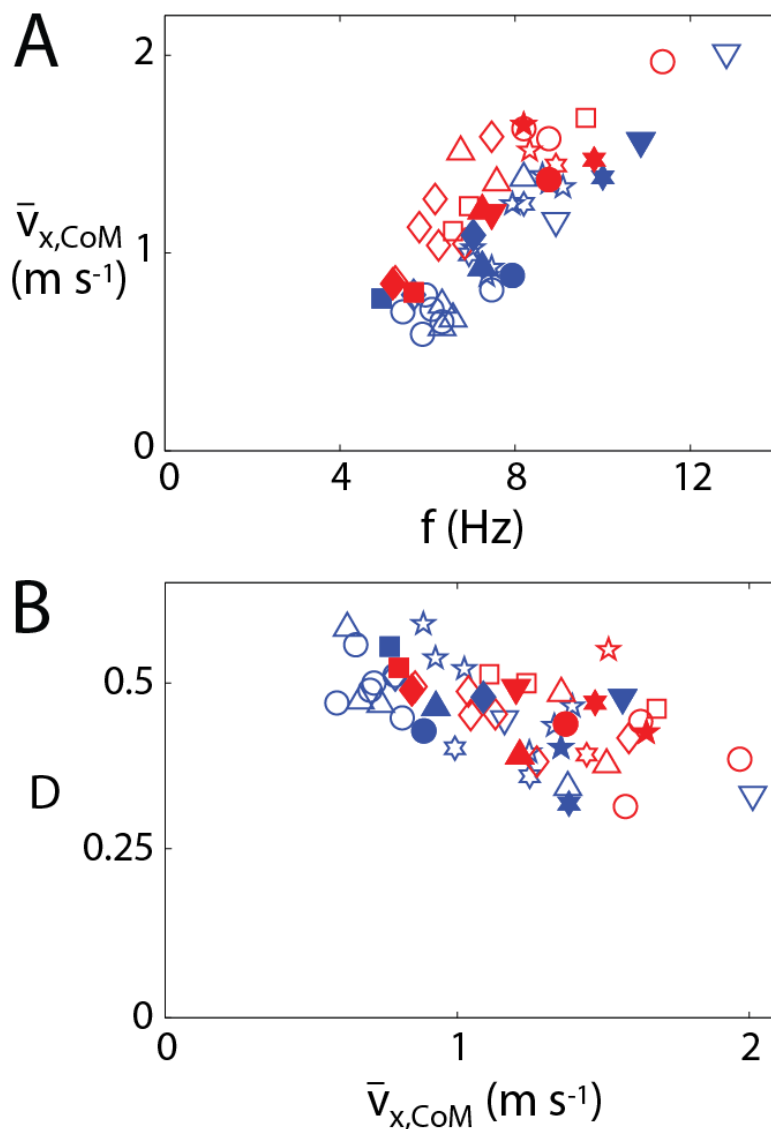
915

916 Fig. 2. Experiments to measure hind limb resilience and granular penetration force. (A)
 917 Experimental setup for hind limb resilience measurements. Dashed foot tracing shows the relaxed,
 918 straight foot right before touchdown. Solid foot tracing shows the hyperextended foot during
 919 ground contact. F , ground reaction force; θ_0 , angle between the ankle and the digit tip in the
 920 relaxed, straight foot; θ_t , angle between the ankle and the digit tip in the hyperextended foot; τ ,
 921 torque about the ankle. (B) Experimental setup for granular penetration force measurements.



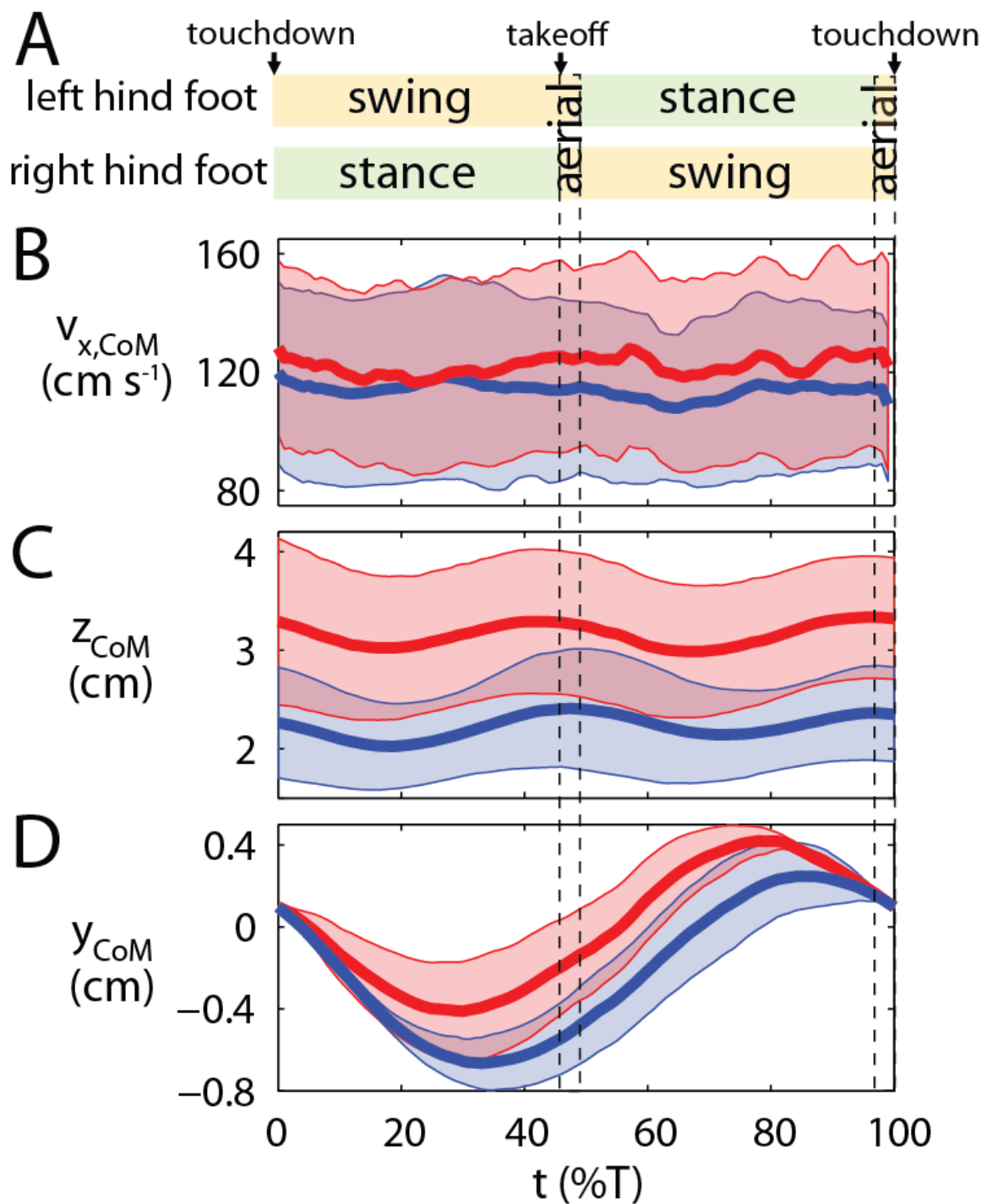
922

923 Fig. 3. Lateral views of representative runs on the solid (A–D) and the granular (F–I) surface (see
 924 Movies 1, 2 in supplementary material). (E,J) Closer views of foot posture at touchdown showing
 925 definition of touchdown foot angle $\theta_{\text{touchdown}}$. Solid lines and curves along the foot indicate hind
 926 foot posture and shape. Note that the lateral camera was oriented at an angle to the x , y , z axes
 927 such that forward ($+x$) direction appeared to point slightly downwards.



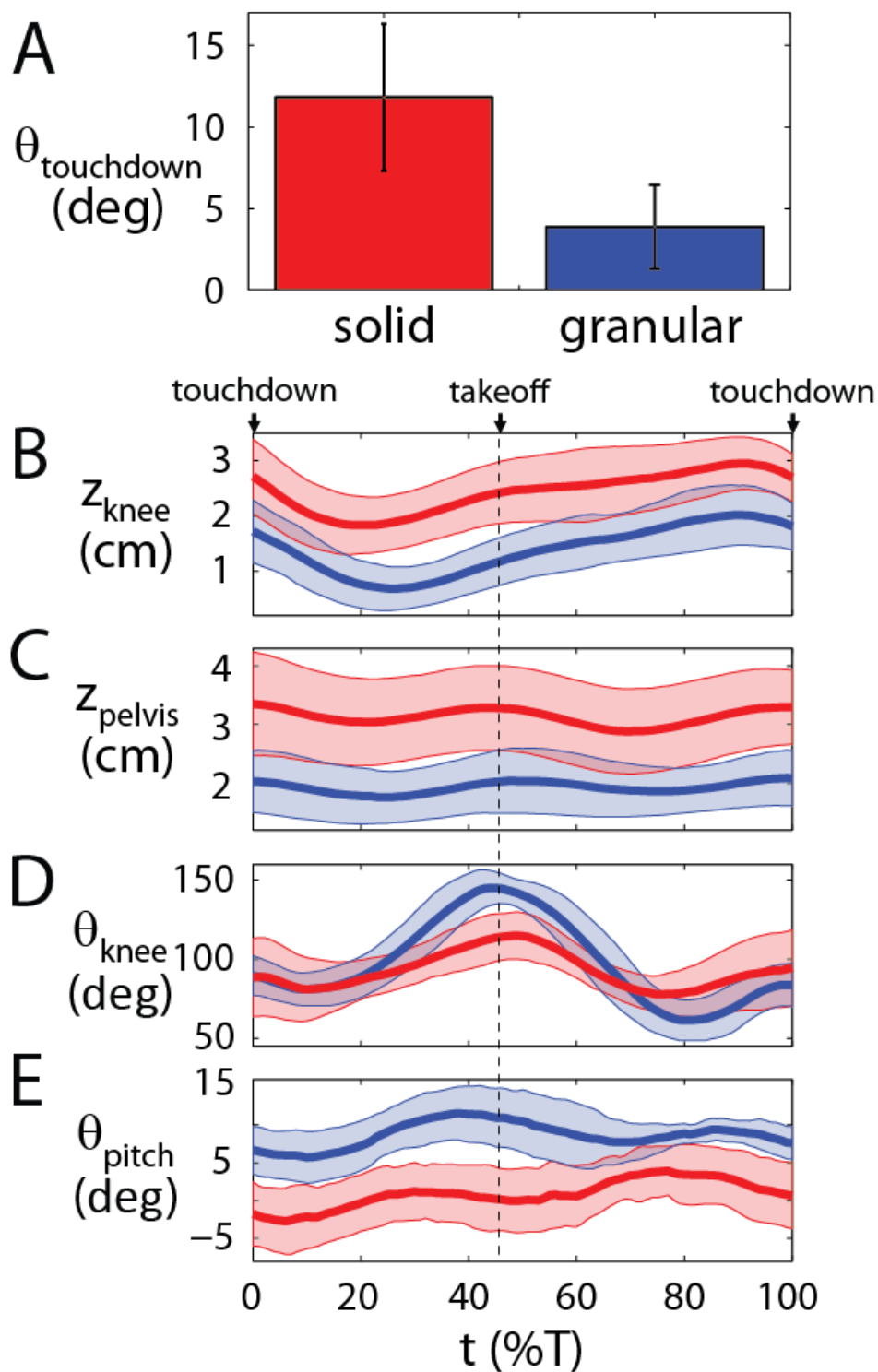
928

929 Fig. 4. Performance and gait on the solid (red) and the granular (blue) surfaces. (A) Average
930 forward speed vs. stride frequency. (B) Duty factor vs. average forward speed. Different symbols
931 represent different individuals. Filled symbols are from the seven representative runs for each of
932 the seven individuals tested on both substrates. Empty symbols are from runs that were not
933 included in the representative data set.



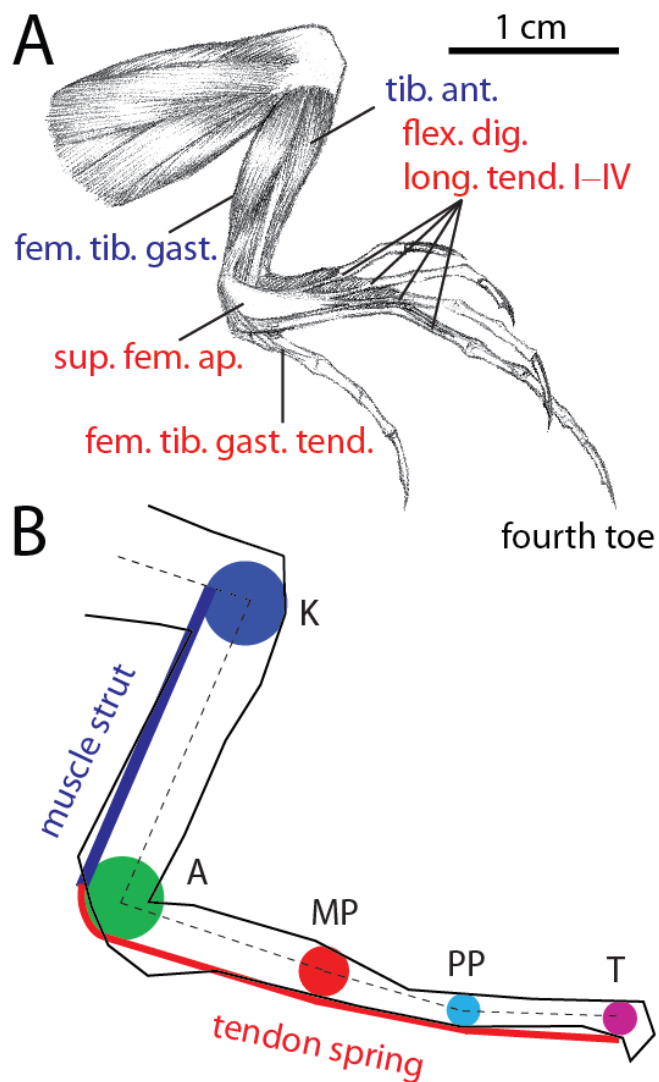
934

935 Fig. 5. Center of mass (CoM) kinematics (mean \pm s.d.) vs. time during a stride on the solid (red)
 936 and the granular (blue) surfaces. (A) Footstep pattern. (B) CoM forward speed. (C) CoM vertical
 937 position. (D) CoM lateral position. See Fig. 1 for definitions of kinematic variables.



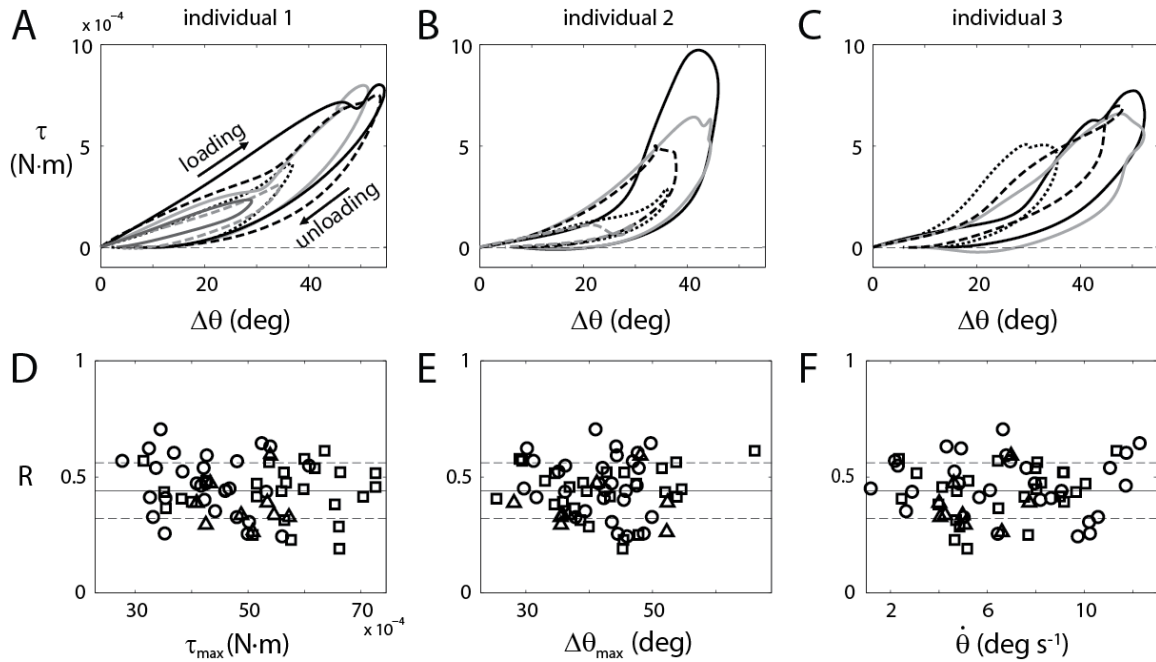
938

939 Fig. 6. Hind foot, hind leg, and trunk kinematics (mean \pm s.d.) vs. time during a stride on the solid
 940 (red) and the granular (blue) surfaces. (A) Touchdown foot angle. (B) Knee height. (C) Pelvis
 941 height. (D) Knee angle. (E) Trunk pitch angle. See Fig. 1 and Fig. 3E,J for definitions of
 942 kinematic variables.



943

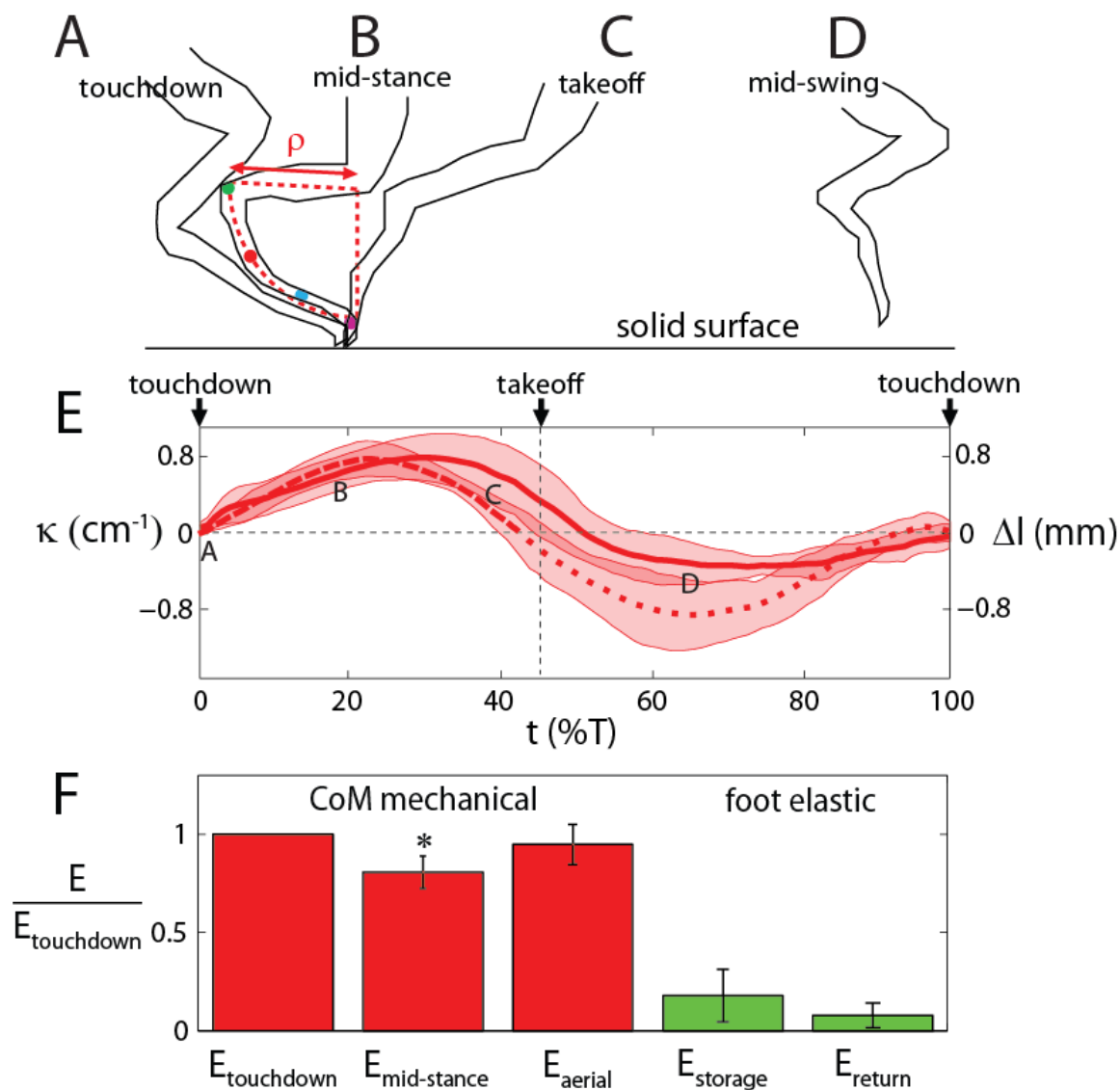
944 Fig. 7. Anatomy and a strut-spring model of the hind limb. (A) Ventral anatomy of a dissected
945 hind limb. Lower hind leg muscles are marked in blue; foot tendons are marked in red. (B) A
946 two-dimensional model of the hind limb. The muscle strut models isometrically contracting lower
947 leg muscles; the tendon spring models foot tendons. The radii of colored circles correspond to
948 measured joint radii.



949
950

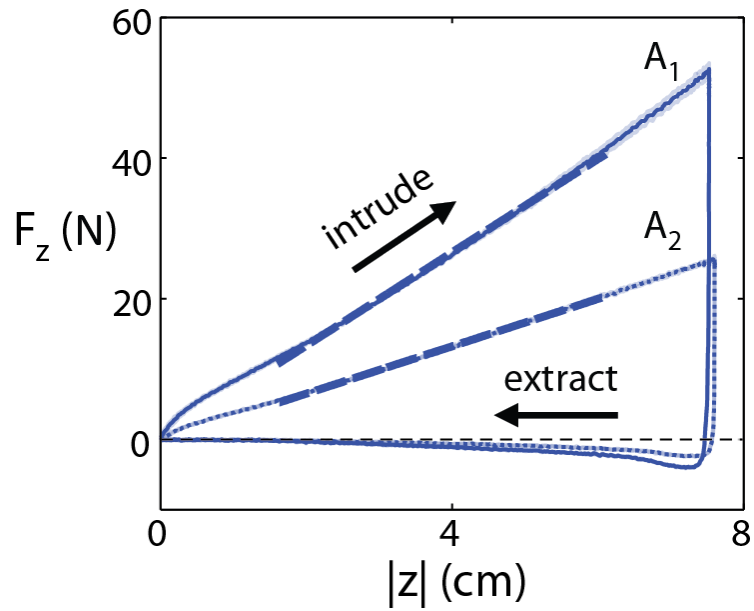
951 Fig. 8. Hind limb resilience. (A–C) Representative passive work loops of the hind foot (measured
952 at the digit tip) from each of the three anesthetized lizards tested. Different curves are from
953 different trials. The area within a work loop is the energy lost within the foot. See Fig. 2A for
954 schematic of experimental setup. (D–F) Hind limb resilience vs. maximal torque, maximal
955 angular displacement, and average loading rate. Different symbols are from different individuals.
956 Solid and dashed lines in (D–F) denote mean \pm s.d.

957



958

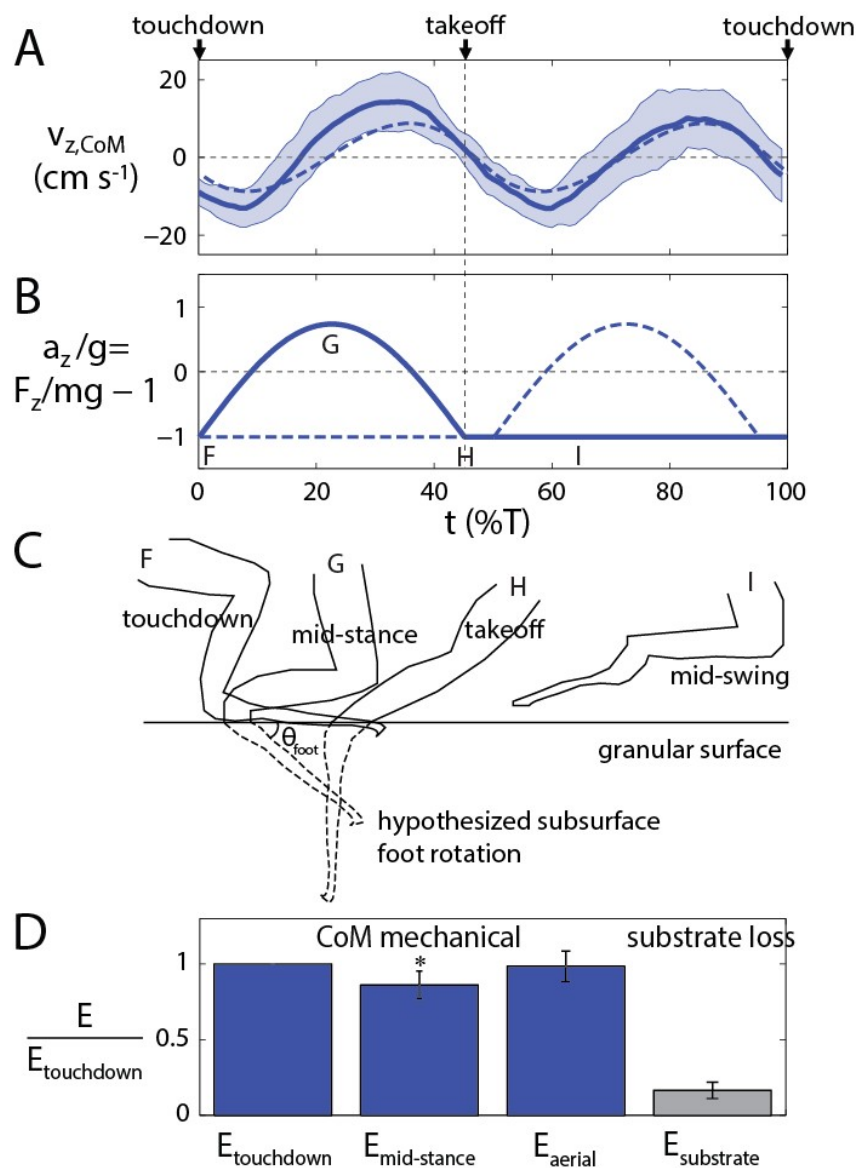
959 Fig. 9. Foot-ground interaction on the solid surface. (A–D) The hind foot shape from the lateral
 960 view of a representative run on the solid surface. (A–D) correspond with (A–D) in Fig. 3. The
 961 hind foot shape in the dorsal view is similar because the sprawl angle of the foot plane is nearly
 962 constant during stance. The diagram in (B) defines the radius of curvature ρ of the foot (see
 963 Appendix). (E) Foot curvature (solid) and tendon spring deformation (dashed) (mean \pm s.d.) vs.
 964 time during a stride on the solid surface. Tendon spring deformation is not meaningful during
 965 swing (dotted) when the muscle strut assumption does not hold. (F) Mechanical energies of the
 966 CoM and elastic energies of the foot (mean \pm s.d.) on the solid surface. All energies are
 967 normalized to the mechanical energy of the CoM at touchdown ($E_{\text{touchdown}}$) for each run. *
 968 indicates that $E_{\text{mid-stance}}$ is significantly different from $E_{\text{touchdown}}$ and E_{aerial} ($P < 0.05$, ANOVA,
 969 Tukey HSD).



970

971 Fig. 10. Granular penetration force (mean \pm s.d.) vs. depth on two plates of different areas: $A_1 =$
972 $7.6 \times 2.5 \text{ cm}^2$ and $A_2 = 3.8 \times 2.5 \text{ cm}^2$. See Fig. 2B for schematic of experimental setup. Dashed
973 lines are linear fits to the data over steady state during penetration using Eqn. (1).

974



975

976 Fig. 11. Foot-ground interaction on the granular surface. (A) CoM vertical speed (mean \pm s.d.) vs.
 977 time during a stride. Solid curve is from experiment. Dashed curve is calculated from the vertical
 978 acceleration from the model. (B) Vertical acceleration vs. time during a stride calculated from the
 979 total vertical ground reaction force F_z on both feet and the animal weight mg . Solid and dashed
 980 curves are the F_z on the two alternating hind feet. (C) Hypothesized subsurface foot rotation in the
 981 sagittal plane. (F–I) correspond with (F–I) in Fig. 3. θ_{foot} , foot angle in the vertical plane. (D)
 982 Mechanical energy of the CoM and the energy loss to the substrate (mean \pm s.d.) during running
 983 on the granular surface. All energies are normalized to the mechanical energy of the CoM at
 984 touchdown ($E_{touchdown}$) for each run. * indicates that $E_{mid-stance}$ is significantly different from
 985 $E_{touchdown}$ and E_{aerial} ($P < 0.05$, ANOVA, Tukey HSD).

986

987 Table 1. Morphological measurements (mean \pm s.d.) of the seven individuals tested in the 3-D
988 kinematics experiments.

SVL (cm)	7.2 \pm 0.6
Mass m (g)	11.0 \pm 2.7
Trunk length (cm)	4.4 \pm 0.4
Pelvic width (cm)	1.4 \pm 0.1
Hind limb length (cm)	6.4 \pm 0.1
Hind foot length (cm)	2.7 \pm 0.1
Femur length (cm)	1.6 \pm 0.2
Tibia length (cm)	2.1 \pm 0.2
Tarsals and metatarsals length (cm)	1.0 \pm 0.1
Fourth toe length (cm)	1.7 \pm 0.1

989

990 Table 2. Gait and kinematic variables (mean \pm s.d.) and statistics using an ANCOVA. *P* values
 991 reported are for substrate effect.

Variable	Solid	Granular	<i>F</i>	<i>P</i>
†Average forward speed $\bar{v}_{x,CoM}$ (m/s)	1.2 \pm 0.3	1.1 \pm 0.3	0.4784	0.5023
Stride frequency <i>f</i> (Hz)	7.5 \pm 1.6	8.1 \pm 2.0	9.9101	0.0319
Duty factor <i>D</i>	0.46 \pm 0.05	0.45 \pm 0.07	0.5032	0.5480
Stride length λ (m)	0.16 \pm 0.02	0.14 \pm 0.02	8.9112	0.0409
Average CoM height \bar{z}_{CoM} (cm)	3.2 \pm 0.7	2.2 \pm 0.5	5.4690	0.0203
Magnitude of CoM vertical oscillations Δz_{CoM} (cm)	0.3 \pm 0.2	0.4 \pm 0.3	3.7031	0.4697
Lowest CoM height z_{CoM} (cm)	3.0 \pm 0.7	2.0 \pm 0.4	7.7544	0.0115
Time of lowest CoM height (<i>T</i>)	0.18 \pm 0.04	0.19 \pm 0.04	0.9696	0.6366
Highest CoM height z_{CoM} (cm)	3.3 \pm 0.7	2.4 \pm 0.6	3.6126	0.0447
Time of highest CoM height (<i>T</i>)	0.44 \pm 0.04	0.48 \pm 0.01	3.0642	0.0325
Magnitude of CoM lateral oscillations Δy_{CoM} (cm)	0.86 \pm 0.19	0.94 \pm 0.23	0.2350	0.5263
Average pelvis height pelvis \bar{z}_{pelvis} (cm)	3.1 \pm 0.7	1.9 \pm 0.5	8.8912	0.0046
Average trunk pitch angle $\bar{\theta}_{pitch}$ (deg)	1 \pm 3	9 \pm 2	19.5282	0.0002
Touchdown knee height z_{knee} (cm)	2.7 \pm 0.7	1.7 \pm 0.6	6.7157	0.0171
Lowest knee height z_{knee} (cm)	1.8 \pm 0.5	0.7 \pm 0.4	15.4261	0.0006
Knee vertical displacement during stance Δz_{knee} (cm)	0.9 \pm 0.2	1.1 \pm 0.4	0.7128	0.3056
Touchdown knee angle θ_{knee} (deg)	88 \pm 25	90 \pm 13	1.2344	0.6713
Lowest knee angle θ_{knee} (deg)	79 \pm 17	79 \pm 10	1.3175	0.7549
Highest knee angle θ_{knee} (deg)	116 \pm 15	150 \pm 8	17.568	0.0001
Knee joint extension during stance $\Delta\theta_{knee}$ (deg)	37 \pm 13	71 \pm 4	18.0994	0.0001
‡Average leg sprawl angle during stance θ_{sprawl} (deg)	40 \pm 1	38 \pm 5	N/A	N/A
Touchdown foot angle $\theta_{touchdown}$ (deg)	12 \pm 4	4 \pm 3	7.6973	0.0032

992 All significant differences ($P < 0.05$) are in bold. Degree of freedom is (2,11) for all variables.

993 † An ANOVA was used to test the effect of substrate on running speed.

994 ‡ A direct comparison was not possible for θ_{sprawl} between substrates because θ_{sprawl} was measured
 995 differently: on the solid surface, leg orientation was measured from the hip to the digit tip; on the
 996 granular surface, leg orientation was measured from the hip to the ankle.

997

998 Table 3. Normalized energetic variables (mean \pm s.d.). All energies were normalized to $E_{\text{touchdown}}$
 999 for each run and averaged over 7 representative runs on each substrate.

Variable	Solid	Granular
Mechanical energy at touchdown $E_{\text{touchdown}}$	1.00 \pm 0.00	1.00 \pm 0.00
Mechanical energy at mid-stance $E_{\text{mid-stance}}$	0.81 \pm 0.08*	0.86 \pm 0.09*
Mechanical energy during aerial phase E_{aerial}	0.95 \pm 0.10	0.99 \pm 0.10
Mechanical energy reduction ΔE_{mech}	0.19 \pm 0.08	0.14 \pm 0.09
Elastic energy storage at mid-stance E_{storage}	0.18 \pm 0.13	N/A
Elastic energy return E_{return}	0.08 \pm 0.06	N/A
Energy loss to substrate $E_{\text{substrate}}$	N/A	0.17 \pm 0.05
Muscle mechanical work W_{muscle}	0.11 \pm 0.10	0.31 \pm 0.10

1000 * indicates significant difference ($P < 0.05$) in the mechanical energy of the CoM at mid-stance
 1001 from that at touchdown and during aerial phase.